Hamiltonian Structure and Statistically Relevant Conserved Quantities for the Truncated Burgers-Hopf Equation

RAFAIL V. ABRAMOV
Rensselaer Polytechnic Institute
Courant Institute
GREGOR KOVAČIČ
Rensselaer Polytechnic Institute
AND
ANDREW J. MAJDA
Courant Institute

Dedicated to Peter Lax in his 75th year

Abstract

In dynamical systems with intrinsic chaos, many degrees of freedom, and many conserved quantities, a fundamental issue is the statistical relevance of suitable subsets of these conserved quantities in appropriate regimes. The Galerkin truncation of the Burgers-Hopf equation has been introduced recently as a prototype model with solutions exhibiting intrinsic stochasticity and a wide range of correlation scaling behavior that can be predicted successfully by simple scaling arguments. Here it is established that the truncated Burgers-Hopf model is a Hamiltonian system with Hamiltonian given by the integral of the third power. This additional conserved quantity, beyond the energy, has been ignored in previous statistical mechanics studies of this equation. Thus, the question arises of the statistical significance of the Hamiltonian beyond that of the energy. First, an appropriate statistical theory is developed that includes both the energy and Hamiltonian. Then a convergent Monte Carlo algorithm is developed for computing equilibrium statistical distributions. The probability distribution of the Hamiltonian on a microcanonical energy surface is studied through the Monte-Carlo algorithm and leads to the concept of statistically relevant and irrelevant values for the Hamiltonian. Empirical numerical estimates and simple analysis are combined to demonstrate that the statistically relevant values of the Hamiltonian have vanishingly small measure as the number of degrees of freedom increases with fixed mean energy. The predictions of the theory for relevant and irrelevant values for the Hamiltonian are confirmed through systematic numerical simulations. For statistically relevant values of the Hamiltonian, these simulations show a surprising spectral tilt rather than equipartition of energy. This spectral tilt is predicted and confirmed independently by Monte Carlo simulations based on equilibrium statistical mechanics together with a heuristic formula for the tilt. On the other hand, the theoretically predicted correlation scaling law is satisfied both for statistically relevant and irrelevant values of the Hamiltonian with excellent accuracy. The results established here for the Burgers-Hopf model are a prototype for similar issues with significant practical importance in much more complex geophysical applications. Several interesting mathematical problems suggested by this study are mentioned in the final section.

Communications on Pure and Applied Mathematics, Vol. LVI, 0001–0046 (2003)

Contents

1 Introduction

Recently Majda and Timofeyev [12, 13] have introduced the Galerkin truncation of the Burgers-Hopf equation as an extremely simple one-dimensional model with complex features in common with vastly more complex and challenging problems in contemporary science ranging from short-term climate prediction for the coupled atmosphere-ocean system to simulating protein folding through molecular dynamics. The model is defined through the finite Fourier series truncation of a real-valued 2π-periodic function f, $P_\Lambda f = f_\Lambda$, with

$$P_\Lambda f = f_\Lambda = \sum_{|k|\le\Lambda} \hat{f}_k e^{ikx}\,, \quad \hat{f}_{-k} = \hat{f}_k^*\,.$$

This model is defined by the Galerkin truncation of the Burgers-Hopf equation,

$$(u_\Lambda)_t + \tfrac{1}{2} P_\Lambda \left(u_\Lambda^2\right)_x = 0\,.$$

Despite its simplicity, solutions of this model with a fairly large number of degrees of freedom, i.e., Λ ranging from 10 to 200, exhibit intrinsic chaos and, more importantly as a model for complex applications, a wide range of scales for the correlations that can be predicted by a simple scaling theory and confirmed numerically (see [12, 13] and Sections 3 and 4 below). These properties make the truncated Burgers-Hopf equation (TBH) an ideal simplified model for testing theories of predictability [9] and stochastic mode reduction [14, 15] designed for vastly more complex applications. Of course, the statistical behavior of TBH, which is the main subject of this study, has nothing to do with the numerical computation of shocks in discontinuous solutions for the inviscid Burgers equation; instead, the TBH is utilized here as a simple model with intrinsic chaos and several conserved quantities in a system with many degrees of freedom.

Solutions of the truncated Burgers-Hopf equations have the three conserved quantities

$$\int u_\Lambda \, dx = M, \quad \text{momentum}, \qquad \int P\big(u_\Lambda^2\big) dx = E, \quad \text{energy},$$
$$\int P\big(u_\Lambda^3\big) dx = H, \quad \text{Hamiltonian}.$$

In references [12] and [13], Majda and Timofeyev developed an equilibrium statistical theory for the truncated Burgers-Hopf equation based solely on the two conserved quantities defined by momentum and energy, M and E alone, with corresponding predictions of equipartition of energy. These predictions were verified with astonishing accuracy for a wide variety of deterministic and random initial data. See Sections 3 and 4 of the present paper for more discussion and amplification on the results from [12] and [13]. The first new contribution in the present paper is developed in Section 2, where the authors establish that the TBH equation is a Hamiltonian system with Hamiltonian $H(u_\Lambda)$ defined by the integral of the third power of u_Λ; in particular, $H(u_\Lambda)$ is a conserved quantity.

The principal goal of this paper is to utilize TBH once again, as a simple model for fundamental issues arising in the statistical behavior of vastly more sophisticated dynamical systems. In a dynamical system with many conserved quantities and intrinsic chaos, which of these conserved quantities are statistically relevant and irrelevant in various regimes of their values? For the TBH model, both the quadratic energy E and the cubic Hamiltonian H are the conserved quantities. Thus, the questions naturally arise regarding whether and when this additional conserved quantity, $H(u_\Lambda)$, is statistically relevant for solutions of the truncated Burgers-Hopf dynamics. Quantifying and answering this question through the symbiotic interaction of mathematical theory, concise numerical algorithms for equilibrium statistical mechanics, and direct simulations is the objective of Sections 3, 4, and 5 of the present paper.

Once again, the truncated Burgers-Hopf equation has a role as a simple model. The issues of statistically relevant and irrelevant conserved quantities discussed in this paper for the truncated Burgers-Hopf equation serve as an elementary model for the same issues in much more complex geophysical applications where these issues have genuinely practical significance ([6, 8, 16, 18, 19]; also see additional references in [19]). To simplify this discussion, we note that inviscid two-dimensional flow possesses, apart from the energy, the infinitely many conserved quantities involving vorticity,

$$\int |\omega|^p = Q_p(\omega)\,,$$

and the statistical relevance of these and related conserved quantities is a hotly debated topic in the applied literature ([6, 8, 19, 16, 18] and references therein). Two of the present authors in a publication in preparation [3] address these issues using the same strategy developed in this paper for the much simpler truncated Burgers-Hopf model on the more complex geophysical models that require other

additional insights, both numerical and mathematical. Next we summarize the contents of the remainder of the paper.

In Section 3, the authors discuss equilibrium statistical mechanics formulations for the truncated Burgers-Hopf equation that include the Hamiltonian $H(u_\Lambda)$ as a conserved quantity. Also, a convergent Monte Carlo algorithm is developed for computing integrals over large-dimensional spheres, utilized here for Λ ranging from 10 to 100. This algorithm is applied for calculating the probability density of the Hamiltonian on a microcanonical energy surface with fixed mean energy as the number of degrees of freedom Λ increases. This probability distribution is roughly self-similar and Gaussian, and peaks sharply around the value $H(u_\Lambda) = 0$ as Λ increases.

Since the Hamiltonian is clearly statistically irrelevant on the subsurface defined by $H(u_\Lambda) = 0$, these facts naturally lead to the concept of statistically relevant and irrelevant values of the Hamiltonian defined in Section 3. It is established through the above empirical facts and a simple small-deviation argument that the statistically relevant values for the Hamiltonian occupy a set of vanishingly small probability as Λ increases for fixed mean energy. All of the initial data, both deterministic and random, utilized by Majda and Timofeyev in references [12] and [13], lie in the statistically irrelevant regime for the Hamiltonian, and this explains why the Hamiltonian played no role in the earlier studies.

In Section 4, systematic numerical simulations are developed for the truncated Burgers-Hopf equation that confirm the role of statistically relevant and irrelevant values for the Hamiltonian. The correlation scaling law proposed in [12] and [13] is confirmed for both statistically relevant and irrelevant values of the Hamiltonian. Despite this fact, for statistically relevant values of the Hamiltonian, there is a tilt in the energy spectrum rather than equipartition of energy. In Section 5, this novel tilt in the spectrum for statistically relevant values of the Hamiltonian is predicted with surprising accuracy by a purely equilibrium statistical Monte Carlo calculation. This agreement between the equilibrium statistical predictions and the direct numerical simulations for the spectral tilt verifies the accuracy of both complementary approaches and also sharply supports the ergodicity of the truncated Burgers-Hopf equation on the intersection of the hypersurfaces, $H = H_0$ and $E = E_0$. Several accessible mathematical analysis problems suggested by this study are mentioned briefly in the concluding discussion.

This paper is dedicated to Peter Lax, who has pioneered the style of research utilized in this paper where mathematical theory, concise scientific computing, and numerical analysis mingle to give insight into a simplified model used as a prototype for vastly more complex systems of interest in contemporary science.

2 Truncated Burgers-Hopf Equation as a Hamiltonian System

We begin with the Burgers-Hopf equation,

$$u_t + uu_x = 0\,, \quad u(x,t) = u(x+2\pi,t)\,. \tag{2.1}$$

It is well known that for smooth solutions the Burgers-Hopf equation (2.1) is Hamiltonian and can in fact be derived via two distinct Hamiltonian structures [17]. We begin this section by briefly reviewing the structure that we will use in the rest of the paper.

We first recall the definition of a Poisson bracket on the space of infinitely smooth periodic functions on the interval $[0, 2\pi]$; see [1, 4]. Given any two functionals $\mathcal{F}[u, u_x, u_{xx}, \dots]$ and $\mathcal{G}[u, u_x, u_{xx}, \dots]$ on this space, a Poisson bracket is defined by the formula

$$\{\mathcal{F}, \mathcal{G}\} \equiv \int_0^{2\pi} dx \frac{\delta \mathcal{F}}{\delta u} J \frac{\delta \mathcal{G}}{\delta u}, \tag{2.2}$$

where $\delta \cdot / \delta u$ denotes the variational derivative. The operator

$$J(u, u_x, u_{xx}, \dots)$$

is called the symplectic operator and must satisfy the following two properties:

- J must be skew-symmetric, so that $\{\mathcal{A}, \mathcal{B}\} = -\{\mathcal{B}, \mathcal{A}\}$ for any two functionals $\mathcal{A}[u, u_x, u_{xx}, \dots]$ and $\mathcal{B}[u, u_x, u_{xx}, \dots]$, and
- J must induce the Jacobi identity

  $$\{\{\mathcal{A}, \mathcal{B}\}, \mathcal{C}\} + \{\{\mathcal{C}, \mathcal{A}\}, \mathcal{B}\} + \{\{\mathcal{B}, \mathcal{C}\}, \mathcal{A}\} = 0$$

  in the Poisson bracket (2.2).

Given a Poisson bracket, an equation of the form

$$u_t = F(u, u_x, u_{xx}, \dots) \tag{2.3}$$

is defined to be Hamiltonian if it can be written as

$$u_t = J(u, u_x, u_{xx}, \dots) \frac{\delta \mathcal{H}[u, u_x, u_{xx}, \dots]}{\delta u}. \tag{2.4}$$

The functional $\mathcal{H}$ is the corresponding Hamiltonian for this equation.

One can easily compute that the evolution of any quantity

$$\mathcal{F}[u, u_x, u_{xx}, \dots]$$

under the dynamics of equation (2.4) obeys the equation

$$\mathcal{F}_t = \{\mathcal{F}, \mathcal{H}\}. \tag{2.5}$$

Two more properties are evident:

- The Hamiltonian is conserved in time, i.e.,

  $$\mathcal{H}_t = \{\mathcal{H}, \mathcal{H}\} = -\{\mathcal{H}, \mathcal{H}\} = 0.$$

- Any functional $\mathcal{C}$ that satisfies

  $$J \frac{\delta \mathcal{C}}{\delta u} \equiv 0 \tag{2.6}$$

  independently of the choice of the function u is conserved regardless of what the Hamiltonian $\mathcal{H}$ is. Such functionals are called *Casimir invariants* and depend only on the operator J.

2.1 A Hamiltonian Representation of the Burgers-Hopf Equation

The Burgers-Hopf equation (2.1) belongs to the class of equations

$$u_t + [f(u)]_x = 0\,. \tag{2.7}$$

Restricted to smooth solutions, any such equation with periodic boundary conditions $u(x,t) = u(x+2\pi,t)$ is Hamiltonian and can be written as

$$u_t = J\frac{\delta \mathcal{H}}{\delta u}\,, \tag{2.8a}$$

where the symplectic operator J and the Hamiltonian $\mathcal{H}$ are given by the formulae

$$J = -2\pi\frac{\partial}{\partial x}\,, \tag{2.8b}$$

$$\mathcal{H} = \int_0^{2\pi} F(u)dx\,, \qquad F_u = f(u)\,, \tag{2.8c}$$

respectively. For periodic u, the symplectic operator J is clearly skew-symmetric and automatically satisfies the Jacobi identity because it does not depend on the function u or its derivatives. The corresponding Poisson bracket is

$$\{\mathcal{F},\mathcal{G}\} = \int_0^{2\pi}\frac{\delta \mathcal{F}}{\delta u}\left(-2\pi\frac{\partial}{\partial x}\right)\frac{\delta \mathcal{G}}{\delta u}\,dx\,. \tag{2.9}$$

For the Burgers-Hopf equation (2.1) we set

$$f(u) = \frac{1}{2}u^2\,,$$

and therefore

$$\mathcal{H} = \frac{1}{12\pi}\int_0^{2\pi} u^3\,dx\,. \tag{2.10}$$

In the context of the Korteweg–de Vries equation, the Hamiltonian structure (2.8) and the Poisson bracket (2.9) were discovered in [7].

The symplectic operator (2.8b) possesses a single Casimir invariant. To show this, we note that the condition that this Casimir invariant must satisfy is

$$\frac{\partial}{\partial x}\frac{\delta \mathcal{C}}{\delta u} = 0\,,$$

that is,

$$\frac{\delta \mathcal{C}}{\delta u} = \text{const}.$$

Since this last equation must be valid for every smooth function u that is inserted in the functional $\mathcal{C}$, the only possible solution can be

$$\mathcal{C} = \text{const}\int_0^{2\pi} u\,dx\,.$$

The particular choice of the constant $1/(2\pi)$ yields

$$\mathcal{C} = \frac{1}{2\pi}\int_0^{2\pi} u\,dx\,, \tag{2.11}$$

which is the momentum of the solution $u(x,t)$.

The generalized equation (2.7) also has infinitely many conserved quantities of the form

$$\frac{\partial}{\partial t}\int_0^{2\pi} g(u)dx = 0\,. \tag{2.12}$$

This can be easily shown by the calculation

$$\begin{aligned}\frac{\partial}{\partial t}\int_0^{2\pi} g(u)dx = \int_0^{2\pi} g_t\,dx = \int_0^{2\pi} g_u u_t\,dx &= -\int_0^{2\pi} g_u f_u u_x\,dx\\ &= -\int_0^{2\pi} G'(u)u_x\,dx\\ &= -\int_0^{2\pi} [G(u)]_x\,dx = 0\,,\end{aligned}$$

with $G(u)$ chosen so that $G'(u) = g_u(u)\,f_u(u)$, with $u(x,t)$ real and periodic.

2.2 Hamiltonian Representation of the Truncated Burgers-Hopf Equation

In this section we explain how the Hamiltonian structure of the Burgers-Hopf equation (2.1) discussed in the previous section induces a Hamiltonian structure on the finite Fourier truncation of this equation. In particular, we will see that both the Hamiltonian (2.10) and the momentum Casimir (2.11) that we find in the truncated system are natural truncations of their counterparts in the original Burgers-Hopf dynamics. We will show below that another conserved quantity, the energy, also survives under truncation.

We begin by denoting the projection operator P_Λ on a finite number $(2\Lambda+1)$ of Fourier modes by

$$P_\Lambda f(x) = f_\Lambda(x) = \sum_{k=-\Lambda}^{\Lambda} \hat{f}_k e^{ikx}\,, \tag{2.13}$$

where

$$\hat{f}_k = \frac{1}{2\pi}\int_0^{2\pi} f(x)e^{-ikx}\,dx$$

is the k^{th} Fourier coefficient of the function $f(x)$. For real functions $f(x)$,

$$\hat{f}_{-k} = \hat{f}_k^*\,.$$

By using the projection operator (2.13), we write the truncated Burgers-Hopf equation as

$$(u_\Lambda)_t + \frac{1}{2}\frac{\partial}{\partial x} P_\Lambda\big(u_\Lambda^2\big) = 0\,. \tag{2.14}$$

This equation is Hamiltonian with the same symplectic structure (2.8) as the original Burgers-Hopf equation (2.1), and the corresponding Hamiltonian is the projection of the original Hamiltonian (2.10) on the first $(2\Lambda + 1)$ Fourier modes,

$$H = \frac{1}{12\pi}\int_0^{2\pi} P_\Lambda\big(u_\Lambda^3\big)dx\,. \tag{2.15}$$

To show this, we first observe that the restriction of the Poisson bracket (2.9) to functionals of the form

$$\mathcal{F}_\Lambda[u_\Lambda, u_{\Lambda x}, u_{\Lambda xx}, \dots] = \int_0^{2\pi} P_\Lambda F(u_\Lambda, u_{\Lambda x}, u_{\Lambda xx}, \dots)dx \tag{2.16}$$

is clearly still a Poisson bracket. Thus all we have to show is that the equation (2.14) has the form (2.8a) with the Hamiltonian (2.15). This is true because

$$\frac{\delta H(u_\Lambda)}{\delta u_\Lambda} = \frac{1}{12\pi}\frac{\partial P_\Lambda(u_\Lambda^3)}{\partial u_\Lambda} = \frac{1}{4\pi} P_\Lambda\big(u_\Lambda^2\big)\,, \tag{2.17}$$

where the last equality is shown by a straightforward calculation.

Since the Poisson bracket for the truncated Burgers-Hopf equation (2.14) is the same as that for the original Burgers-Hopf equation (2.1), it possesses the same momentum Casimir invariant, which in the appropriate projected space reads

$$C = \frac{1}{2\pi}\int_0^{2\pi} u_\Lambda\, dx\,. \tag{2.18}$$

The projected Burgers-Hopf equation (2.14) possesses one more conserved quantity, namely, the *energy*

$$E = \frac{1}{4\pi}\int_0^{2\pi} P_\Lambda\big(u_\Lambda^2\big)dx\,. \tag{2.19}$$

In order to see that the energy is indeed conserved, we compute its Poisson bracket with the Hamiltonian (2.15) to obtain

$$\begin{aligned}\{E, H\} &= -\int_0^{2\pi} \frac{1}{2\pi} u_\Lambda \frac{\partial}{\partial x}\frac{1}{2} P_\Lambda\big(u_\Lambda^2\big)dx \\ &= \int_0^{2\pi} \frac{1}{4\pi} P_\Lambda\big(u_\Lambda^2\big)\frac{\partial u_\Lambda}{\partial x}\,dx = \int_0^{2\pi} \frac{1}{12\pi}\frac{\partial P_\Lambda(u_\Lambda^3)}{\partial x}\,dx = 0\,,\end{aligned}$$

where in the last formula we utilized (2.17).

Since no shocks can develop in a finite truncation, the Hamiltonian (2.15), the momentum (2.18), and the energy (2.19) are conserved by the dynamics of the truncated Burgers-Hopf equations (2.14) for all times.

While, for a smooth solution, the original Burgers-Hopf equation (2.1) possesses an infinite family of conserved quantities, this appears not to be the case for the projected Burgers-Hopf equation (2.14). In fact, we find that no projected powers of u except for the first three just described are conserved, that is,

$$\left\{P_\Lambda\left(u_\Lambda^n\right), H\right\} \neq 0\,, \quad n > 3\,.$$

To show this, we follow the sequence of equalities that begins with the antisymmetry of the Poisson bracket,

$$\int_0^{2\pi} \frac{\partial P_\Lambda(u_\Lambda^n)}{\partial u_\Lambda} \frac{\partial}{\partial x} \frac{\partial P_\Lambda(u_\Lambda^3)}{\partial u_\Lambda}\, dx = -\int_0^{2\pi} \frac{\partial P_\Lambda(u_\Lambda^3)}{\partial u_\Lambda} \frac{\partial}{\partial x} \frac{\partial P_\Lambda(u_\Lambda^n)}{\partial u_\Lambda}\, dx,$$

$$\int_0^{2\pi} P_\Lambda\left(u_\Lambda^{n-1}\right) \frac{\partial}{\partial x} P_\Lambda\left(u_\Lambda^2\right) dx = -\int_0^{2\pi} P_\Lambda\left(u_\Lambda^2\right) \frac{\partial}{\partial x} P_\Lambda\left(u_\Lambda^{n-1}\right) dx\,,$$

$$2\int_0^{2\pi} P_\Lambda\left(u_\Lambda^{n-1}\right) P_\Lambda\left(u_\Lambda \frac{\partial u_\Lambda}{\partial x}\right) dx = -(n-1)\int_0^{2\pi} P_\Lambda\left(u_\Lambda^2\right) P_\Lambda\left(u_\Lambda^{n-2} \frac{\partial u_\Lambda}{\partial x}\right) dx\,. \tag{2.20}$$

On the other hand, if the Poisson bracket of two quantities vanishes, it is symmetric; therefore

$$2\int_0^{2\pi} P_\Lambda\left(u_\Lambda^{n-1}\right) P_\Lambda\left(u_\Lambda \frac{\partial u_\Lambda}{\partial x}\right) dx = (n-1)\int_0^{2\pi} P_\Lambda\left(u_\Lambda^2\right) P_\Lambda\left(u_\Lambda^{n-2} \frac{\partial u_\Lambda}{\partial x}\right) dx\,. \tag{2.21}$$

We can see that, in general, equations (2.20) and (2.21) cannot be satisfied simultaneously unless $n = 1,\ 2,$ or 3.

Before concluding this section, we observe that Galilean invariance leads to a useful symmetry of the truncated Burgers-Hopf equations (2.14) (which obviously holds for the original Burgers-Hopf equations (2.1)). In particular, let $\hat{u}_0$ denote the average of the given solution function $u_\Lambda(x,t)$ in the interval $0 < x < 2\pi$; i.e.,

$$\hat{u}_0 = \frac{1}{2\pi}\int_0^{2\pi} u_\Lambda(x,t)dx\,.$$

In other words, $\hat{u}_0$ equals the zeroth Fourier coefficient of $u_\Lambda(x,t)$ and also equals the momentum Casimir invariant $C[u_\Lambda]$ in (2.18). Therefore, it is independent of the time t. Clearly, since $u_\Lambda(x,t)$ is real, then so is $\hat{u}_0$. Let

$$v_\Lambda(x,t) = u_\Lambda(x,t) - \hat{u}_0\,.$$

Then

$$C[v_\Lambda]\,, \quad E[v_\Lambda] = E[u_\Lambda] - \frac{1}{2}\left|\hat{u}_0\right|^2\,, \quad H[v_\Lambda] = H[u_\Lambda] - \hat{u}_0 E[u_\Lambda] + \frac{1}{3}\hat{u}_0^3\,,$$

and equations (2.14) become

$$(v_\Lambda)_t + \hat{u}_0 (v_\Lambda)_x + \frac{1}{2}\frac{\partial}{\partial x} P_\Lambda\big(v_\Lambda^2\big) = 0\,.$$

The shift of the time variable $t \to t - \hat{u}_0 x$ transforms this equation back into

$$(v_\Lambda g)_t + \frac{1}{2}\frac{\partial}{\partial x} P_\Lambda\big(v_\Lambda^2\big) = 0\,,$$

that is, equation (2.14). This argument shows that with no loss of generality we can consider solutions $u_\Lambda(x,t)$ with zero mean.

We remark here that the construction given above establishes that the truncated Burgers-Hopf equation in (2.14) is a Hamiltonian system with (2.13) replaced by any arbitrary finite-dimensional projection P. However, here we always use P_Λ in (2.13).

2.3 Hamiltonian Representation of the Truncated Burgers-Hopf Equation in Spectral Space

In the spectral space of Fourier coefficients, the Hamiltonian equation (2.4) assumes the form

$$\frac{\partial \hat{u}_k}{\partial t} = \sum_{k'=-\infty}^{\infty} \hat{J}_{kk'} \frac{\partial \mathcal{H}}{\partial \hat{u}_{k'}^*}\,. \tag{2.22}$$

Here $\hat{u}_k$ is the k^{th} Fourier coefficient, which we recall satisfies the reality condition

$$\hat{u}_k = \hat{u}_{-k}^*\,, \tag{2.23}$$

$\mathcal{H}$ is the Hamiltonian written in spectral space, and $\hat{J}$ is the infinite symplectic matrix

$$\hat{J}_{kk'} = \left(\frac{\delta \hat{u}_k}{\delta u}\right) J \left(\frac{\delta \hat{u}_{k'}}{\delta u}\right)^\dagger,$$

with † denoting the Hermitian conjugate operator. The operator J is the original symplectic operator in physical space.

Transforming the Hamiltonian representation (2.8) and (2.10) for the Burgers-Hopf equation (2.1) into the above-described spectral form, we find

$$\begin{aligned} \hat{J}_{kk'} &= \left(\frac{\delta \hat{u}_k}{\delta u}\right) J \left(\frac{\delta \hat{u}_{k'}}{\delta u}\right)^\dagger \qquad \text{(2.24a)} \\ &= -\int_0^{2\pi} \frac{1}{2\pi} e^{-ikx} 2\pi \frac{\partial}{\partial x} \frac{1}{2\pi} e^{ik'x}\, dx = -ik'\delta_{k'}^k\,, \\ \mathcal{H} &= \frac{1}{12\pi}\int_0^{2\pi} u^3\, dx = \frac{1}{12\pi} \sum_{k_1,k_2,k_3} \hat{u}_{k_1}\hat{u}_{k_2}\hat{u}_{k_3} \int_0^{2\pi} e^{i(k_1+k_2+k_3)x}\, dx \\ &= \frac{1}{6} \sum_{k_1+k_2+k_3=0} \hat{u}_{k_1}\hat{u}_{k_2}\hat{u}_{k_3}\,. \qquad \text{(2.24b)} \end{aligned}$$

Here $\delta^k_{k'}$ denotes the Kronecker delta.

In the previous section, we have shown that the truncation (2.14) that restricts the equation (2.1) to its first $(2\Lambda+1)$ Fourier modes is Hamiltonian with the Hamiltonian function (2.15). Projecting the above results in equations (2.24) onto the first $(2\Lambda + 1)$ Fourier modes yields the truncated symplectic matrix as

$$\hat{J}_{kk'} = -ik'\delta^k_{k'}\,, \quad |k|, |k'| \leq \Lambda\,, \tag{2.25}$$

and the spectral representation of the Hamiltonian (2.15) as

$$H = \frac{1}{6} \sum_{\substack{k_1+k_2+k_3=0 \\ |k_1|,|k_2|,|k_3|\leq\Lambda}} \hat{u}_{k_1}\hat{u}_{k_2}\hat{u}_{k_3}\,. \tag{2.26}$$

Equation (2.14) thus becomes

$$\frac{\partial \hat{u}_k}{\partial t} = -\frac{ik}{2} \sum_{\substack{|k|,|k'|\leq\Lambda \\ |k-k'|\leq\Lambda}} \hat{u}_{k-k'}\hat{u}_{k'} = -ik\frac{\partial H}{\partial \hat{u}^*_k}\,. \tag{2.27}$$

The projected momentum Casimir invariant (2.18) in the spectral representation assumes the particularly simple form

$$C = \hat{u}_0\,, \tag{2.28}$$

and the conserved energy (2.19) is transformed into

$$E = \frac{1}{2}\sum_{|k|\leq\Lambda} \hat{u}_k\hat{u}_{-k} = \frac{1}{2}\sum_{|k|\leq\Lambda} |\hat{u}_k|^2 = \frac{|\hat{u}_0|^2}{2} + \sum_{k=1}^{\Lambda} \left|\hat{u}_k\right|^2\,. \tag{2.29}$$

The last two equalities in this formula are true because of the reality condition (2.23).

3 Equilibrium Statistical Mechanics for the Truncated Burgers-Hopf Equation

3.1 Gibbs Ensemble for the Energy

In order to set up an equilibrium statistical mechanics theory of the truncated Burgers-Hopf equations (2.27), we first need to establish that they satisfy the Liouville property. For a system of real ordinary differential equations,

$$\dot{\vec{w}} = \vec{F}(\vec{w}) \tag{3.1}$$

with $\vec{w} = (w_1, w_2, \ldots, w_N)$ and $\vec{F}(\vec{w}) = (F_1(\vec{w}), F_2(\vec{w}), \ldots, F_N(\vec{w}))$, the Liouville property is the requirement that the divergence of the vector field $\vec{F}(\vec{w})$ vanish, that is,

$$\nabla \cdot \vec{F}(\vec{w}) = \sum_{k=1}^{N} \frac{\partial F_k(\vec{w})}{\partial w_k} = 0\,. \tag{3.2}$$

For equations (2.27), we establish the Liouville property as follows: We assume with no loss of generality as at the end of Section 2.2 that $\hat{u}_0 = 0$. We let $N = 2\Lambda$ and use the vector notation

$$\vec{w} = (w_1, w_2, \ldots, w_{2\Lambda}), \quad \hat{u}_k = w_{2k-1} + i w_{2k}, \quad k = 1, 2, \ldots, \Lambda, \tag{3.3}$$

to rewrite equations (2.27) in their real form as

$$\dot{w}_{2k-1} = A_k(\vec{w}), \quad \dot{w}_{2k} = B_k(\vec{w}).$$

Then, by using (2.27), we find

$$\frac{\partial A_k}{\partial w_{2k-1}} + \frac{\partial B_k}{\partial w_{2k}} = -ik\frac{\partial^2 H}{\partial \hat{u}_k \partial \hat{u}_k^*} + ik\frac{\partial^2 H}{\partial \hat{u}_k^* \partial \hat{u}_k} = 0.$$

After summing on k, the Liouville property (3.2)

$$\sum_{k=1}^{\Lambda} \left(\frac{\partial A_k}{\partial w_{2k-1}} + \frac{\partial B_k}{\partial w_{2k}} \right) = 0$$

follows. (See also [12] for a direct derivation not involving the Hamiltonian structure.)

Densities on $\mathbb{R}^N$ of probability measures for statistical ensembles of solutions of the equations (3.1) satisfy the Liouville equation,

$$\frac{\partial f}{\partial t} + \nabla \cdot [f \vec{F}(\vec{w})] = 0, \qquad f\big|_{t=0} = f_0, \tag{3.4}$$

where f_0 is the density of the initial probability measure and thus satisfies the conditions

$$f_0 \geq 0 \quad \text{and} \quad \int_{\mathbb{R}^N} f_0(\vec{w}) d\vec{w} = 1.$$

Because of the Liouville property (3.2), any function $G(K)$ of any conserved quantity K of the equations (3.1) must necessarily be a stationary solution of the Liouville equation (3.4).

For the truncated Burgers-Hopf equation (2.27), the discussion of the previous paragraph implies that any function of the momentum C in (2.28), the energy E in (2.29), and the Hamiltonian H in (2.26) is the density of a stationary probability measure for statistical ensembles of its solutions, provided that it can be normalized. In particular, this is true for the densities G_β of the energy-based Gibbs measures,

$$G_\beta = C_\beta e^{-\beta E} = C_\beta e^{-\beta |\vec{w}|^2} = C_\beta \exp\left(-\beta \sum_{k=1}^{\Lambda} |\hat{u}_k|^2 \right), \quad \beta > 0, \tag{3.5}$$

where β is the "inverse temperature," $\vec{w}$ is the vector introduced in (3.3), and

$$|\vec{w}| = \left(\sum_{j=1}^{2\Lambda} w_j^2 \right)^{1/2} \tag{3.6}$$

is the length of the vector $\vec{w}$. It is known [11] that the measures in (3.5) are the unique densities that maximize over all the probability densities the information theoretic entropy,

$$S(p) = -\int_{\mathbb{R}^N} p(\vec{w}) \ln p(\vec{w}) d\vec{w}\,, \quad p > 0\,, \quad \int_{\mathbb{R}^N} p(\vec{w}) d\vec{w} = 1\,,$$

subject to the constraint

$$\bar{E} = \int_{\mathbb{R}^N} E(\vec{w}) p(\vec{w}) d\vec{w}\,.$$

Here $\bar{E}$ is a positive constant representing the mean value of the energy E over the distribution $p(\vec{w})$, and the inverse temperature β is the Lagrange multiplier associated with the maximization problem. The energy-based Gibbs measure (3.5) predicts that the energy should be equipartitioned among all the Fourier modes, and that the mean energy per mode should be

$$\bar{E}_{p/m}(\Lambda) = \frac{\bar{E}}{2\Lambda} = \frac{1}{2\beta}\,. \tag{3.7}$$

In direct numerical simulations, the stationary probability measure is sampled by following long-time trajectories. If the system is ergodic, then given an initial time T_0 and a function $g(\hat{u}_{k_1}, \hat{u}_{k_2}, \ldots, \hat{u}_{k_j})$, its expected value with respect to the measure that is being sampled equals its time average,

$$\langle g \rangle = \int_{\mathbb{R}^N} g(\vec{w}) p(\vec{w}) d\vec{w} = \frac{1}{T} \int_{T_0}^{T+T_0} g\big(\hat{u}_{k_1}(t), \hat{u}_{k_2}(t), \ldots, \hat{u}_{k_j}(t)\big) dt \tag{3.8}$$

in the limit $T \to \infty$, where T is the length of the averaging window. In numerical simulations, the times T and T_0 are fixed at a sufficiently large value so that the numbers on the right-hand side of (3.8) exhibit numerical convergence for the desired functionals g. In particular, the mean energy of the k^{th} mode $\hat{u}_k$ is computed as

$$\frac{1}{2}\big\langle |\hat{u}_k|^2 \big\rangle = \frac{1}{2T} \int_{T_0}^{T+T_0} \big|\hat{u}_k(t)\big|^2 dt\,, \tag{3.9}$$

and the temporal correlation function $c_k(\tau)$ of the k^{th} mode as

$$c_k(\tau) = \frac{1}{T\langle |\hat{u}_k|^2 \rangle} \int_{T_0}^{T+T_0} \big(\hat{u}_k(t) - \langle \hat{u}_k \rangle\big)\big(\hat{u}_k(t+\tau) - \langle \hat{u}_k \rangle\big)^* dt\,. \tag{3.10}$$

By using (3.10), we also define the correlation time T_k for the k^{th} Fourier mode as

$$T_k = \int_0^\infty |c_k(\tau)| d\tau\,. \tag{3.11}$$

In [12, 13], for the truncated Burgers-Hopf equations (2.27), the energy equipartition prediction (3.7) that follows from the energy-based Gibbs measure (3.5) was

verified with remarkable accuracy when compared with the computed mean energy per mode in (3.9) for a wide variety of deterministic and random initial data. This was a severe test, since only the microcanonical statistics for an individual trajectory of the equations (2.27) were sampled rather than a Monte Carlo average over a large number of random initial data as given by the energy-based Gibbs ensemble. In addition, a remarkable correlation scaling theory was developed in [12, 13], which states that the correlation time T_k in (3.11) is proportional to the eddy turnover time,

$$T_k = C_0 \frac{\sqrt{\beta}}{|k|}, \quad 1 \le |k| \le \Lambda, \tag{3.12}$$

with a universal proportionality constant C_0. The results of [12, 13] also show excellent agreement between the correlation times computed numerically by using formula (3.11) and those predicted analytically from formula (3.12) with the constant C_0 chosen to exactly match the correlation time for the mode with $k = 1$.

In most large Hamiltonian systems, the energy and the Hamiltonian are one and the same, and the energy-based Gibbs measure (3.5) is the canonical Gibbs measure of the system. In the truncated Burgers-Hopf equation (2.27), however, this is not the case. The energy E is not the Hamiltonian of the system. Instead, the Hamiltonian is the cubic function H in (2.26). A question thus arises as to the role of this Hamiltonian in the invariant measure for the statistical mechanics of the equation (2.27), in the shape of the correlation functions (3.10), and in the correlation scaling law prediction (3.12). We begin addressing this question in the next section and address it again in Sections 4 and 5.

3.2 Mixed Microcanonical Energy and Canonical Hamiltonian Ensembles

The truncated Burgers-Hopf equations (2.14), or equivalently (2.27), possess three conserved quantities: the momentum Casimir C in (2.28), the energy E in (2.29), and the Hamiltonian H in (2.26). In this section, we address the relevance of these quantities for the equilibrium statistical mechanics of the equations (2.14). By the argument made at the end of Section 2.2, it is clear that the Casimir C can be ignored completely, because, by a simple coordinate change, any solution of equations (2.14) can be mapped into a solution of the same set of equations (2.14) for which $C = 0$. Thus, from now on, we will always assume that every solution $u_\Lambda(x, t)$ of the truncated Burgers-Hopf equations (2.14) that we will investigate has zero mean, that is, its zeroth Fourier coefficient $\hat{u}_0$ vanishes. We therefore turn our attention to the relevance of the Hamiltonian H in (2.26).

In this section, we present a number of numerical and analytical arguments that classify the values of the Hamiltonian H in (2.26) as "typical" and "atypical." While the precise definition is given at the very end of this section, roughly speaking, typical values of the Hamiltonian are those that are the most likely to

be attained along randomly chosen trajectories. The computational results described in Section 4 put forth strong numerical evidence that the typical values of the Hamiltonian H are irrelevant for the statistical mechanics associated with the corresponding solutions of the truncated Burgers-Hopf equation (2.27) in the sense that these solutions exhibit the equipartition energy spectrum in (3.9) and an essentially universal correlation structure by obeying the scaling law (3.12) and exhibiting the same structure for the correlation functions (3.10). On the other hand, our numerical results show that the trajectories of (2.27) with atypical values of the Hamiltonian H exhibit a considerable tilt of the energy spectrum, as well as significant oscillations of the correlation functions (3.10) while retaining the overall correlation scaling law in (3.12). An explanation and quantitative prediction through equilibrium statistical mechanics of the tilt in this spectrum for atypical values is developed in Section 5.

In order to set up an equilibrium statistical mechanics theory for the truncated Burgers-Hopf equations (2.27), we first need to choose an appropriate stationary probability measure for statistical ensembles of solutions. In particular, we need to take into account the fact that equations (2.27) possess two conserved quantities, the energy E in (2.29) and the Hamiltonian H in (2.26), so that the motion of trajectories is confined to the joint isosurfaces of these two conserved quantities. If the Hamiltonian H in (2.26) were a convex function of its arguments, the natural guess for this stationary probability measure would be the canonical distribution in both the energy and the Hamiltonian with the density

$$
\begin{aligned}
G_{\beta,\theta} &= C_{\beta,\theta} e^{-\beta E - \theta H} \\
&= C_{\beta,\theta} \exp\left(-\beta \sum_{k=1}^{\Lambda} |\hat{u}_k|^2 - \frac{\theta}{6} \sum_{k_1+k_2+k_3=0} \hat{u}_{k_1} \hat{u}_{k_2} \hat{u}_{k_3} \right).
\end{aligned}
\tag{3.13}
$$

Here $\beta > 0$ and $\theta > 0$ are two constants, an "inverse temperature" and a "chemical potential." However, formula (3.13) cannot possibly represent a probability density, since its integral over the phase space diverges due to the sign-indefiniteness of the Hamiltonian H.

Instead, the correct route is suggested by the fact that all the simulations are performed microcanonically by following long-time trajectories. In particular, the energy E is kept constant during each simulation. Therefore, in order to study which values of the Hamiltonian H are relevant for the statistical mechanics, we may restrict our attention to fixed-energy isosurfaces. Since equation (2.29) shows that these are spheres, they are compact, and therefore we can use the canonical distribution of the Hamiltonian confined to one of these spheres without fear that the integral of its density will diverge. The statistical mechanical ensemble that we thus obtain is the mixed microcanonical energy and canonical Hamiltonian ensemble. Next, we will describe it in detail as well as justify its use more precisely.

Microcanonical Energy Ensemble

We begin by recalling the microcanonical energy distribution, given by the uniform measure $d\nu_{\bar{E},\Lambda}$ on the $(2\Lambda - 1)$–dimensional sphere $S_{\bar{E},\Lambda}$ of fixed energy in the 2Λ-dimensional real space with coordinates $\vec{w} = (w_1, w_2, \ldots, w_{2\Lambda})$ as in (3.3),

$$S_{\bar{E},\Lambda} = \left\{ \vec{w} : |\vec{w}|^2 = E(\vec{w}) = \sum_{k=1}^{\Lambda} |\hat{u}_k|^2 = \bar{E} \right\}. \tag{3.14}$$

Here $|\vec{w}|$ is the Euclidean length of the vector $\vec{w}$ given in formula (3.6), the radius of this sphere $S_{\bar{E},\Lambda}$ is $R = |\vec{w}| = \sqrt{\bar{E}}$, and the energy $E(\vec{w}) = |\vec{w}|^2 = \sum_{k=1}^{\Lambda} |\hat{u}_k|^2$ is given by (2.29) with $\hat{u}_0 = 0$. The microcanonical energy distribution is given by the formula

$$d\nu_{\bar{E},\Lambda} = [\mathcal{A}(S_{\bar{E},\Lambda})]^{-1} \delta(E(\vec{w}) - \bar{E}) dw_1\, dw_2 \cdots dw_{2\Lambda}\,, \tag{3.15}$$

where $\mathcal{A}(S_{\bar{E},\Lambda})$ is the area of the $(2\Lambda - 1)$–dimensional sphere $S_{\bar{E},\Lambda}$.

Mixed Microcanonical Energy and Canonical Hamiltonian Ensembles

In order to find the distribution of the cubic Hamiltonian H (2.26) on the sphere $S_{\bar{E},\Lambda}$ of fixed energy in (3.14) and subsequently classify the typical and atypical values of H, we first ask what is the least biased probability measure on $S_{\bar{E},\Lambda}$ that gives the effect of the Hamiltonian (2.26) given its mean value $\bar{H}$. A standard argument [11, 16] yields the above-mentioned mixed canonical-microcanonical measure

$$G_{\bar{E},\Lambda,\theta} = \frac{e^{-\theta H(\vec{w})}\, d\nu_{\bar{E},\Lambda}}{\int_{S_{\bar{E},\Lambda}} e^{-\theta H(\vec{w})}\, d\nu_{\bar{E},\Lambda}}\,, \quad \theta > 0\,, \tag{3.16}$$

where θ is again an "inverse temperature."

Probability Distribution of the Hamiltonian on the Microcanonical Energy Surface

To classify the values of the Hamiltonian H on the energy surface $S_{\bar{E},\Lambda}$ as typical or atypical, we need to compute and study the probability measure

$$\mathrm{Prob}_{\bar{E},\Lambda}\{\alpha < H(\vec{w}) < \beta\} = \int_{\alpha}^{\beta} p_{\bar{E},\Lambda}(\lambda) d\lambda \tag{3.17}$$

that describes the distribution of the values of the Hamiltonian H on the sphere of constant energy $S_{\bar{E},\Lambda}$.

Monte Carlo algorithm for generating a uniformly distributed sequence of points on the energy sphere. Now we describe a Monte Carlo algorithm for generating a set of points uniformly distributed on the constant-energy sphere $S_{\bar{E},\Lambda}$

in (3.14) for numerical quadrature of integrals on $S_{\bar{E},\Lambda}$ for large values of Λ between 10 and 100. Here we use this algorithm to compute the Hamiltonian probability distribution function $p_{\bar{E},\Lambda}(\lambda)$ in (3.17) to give us a natural rough classification of values of the Hamiltonian into typical and atypical ones. We also use this procedure extensively in Section 5. Since a detailed reference does not seem to be available in the literature, we describe this algorithm in some detail below.

We begin by describing a number of geometric properties of the uniform measure (3.15) on the fixed-energy sphere $S_{\bar{E},\Lambda}$ that enable us to construct the desired Monte Carlo algorithm. First, we recall that the uniform measure $\nu_{\bar{E},\Lambda}$ in formula (3.15) on the sphere $S_{\bar{E},\Lambda}$ is characterized by the property that

$$\int_{S_{\bar{E},\Lambda}} \varphi\left(\sqrt{\bar{E}}\frac{\vec{w}}{|\vec{w}|}\right) d\nu_{\bar{E},\Lambda} = [\mathcal{A}(S_{\bar{E},\Lambda})]^{-1} \int_{\mathbb{R}^{2\Lambda}} \varphi(\vec{w})\delta(E(\vec{w}) - \bar{E}) dw_1\, dw_2 \cdots dw_{2\Lambda} \tag{3.18}$$

for any function φ continuous on the sphere $S_{\bar{E},\Lambda}$. Here $\mathcal{A}(S_{\bar{E},\Lambda})$ is the area of the $(2\Lambda - 1)$–dimensional sphere $S_{\bar{E},\Lambda}$.

Next, we recall that the normalized surface measure (3.15) is the unique probability measure on the energy sphere $S_{\bar{E},\Lambda}$ that is invariant under all rotations; i.e.,

$$\int_{S_{\bar{E},\Lambda}} \varphi(\mathcal{O}\vec{w}) d\nu_{\bar{E},\Lambda} = \int_{S_{\bar{E},\Lambda}} \varphi(\vec{w}) d\nu_{\bar{E},\Lambda} \tag{3.19}$$

for any rotation matrix $\mathcal{O}$. (Recall that a rotation matrix is any orthogonal transformation $\mathcal{O}$ with determinant 1, that is, $\mathcal{O}\vec{w} \cdot \mathcal{O}\vec{v} = \vec{w} \cdot \vec{v}$ and $\det \mathcal{O} = 1$.)

Thus, we have the following:

CLAIM 1 *If a sequence of measures converges to a measure ν with the property that*

- *ν is supported on the energy sphere $S_{\bar{E},\Lambda}$ in* (3.14)*, and*
- *$\int_{S_{\bar{E},\Lambda}} \varphi(\mathcal{O}\vec{w}) d\nu = \int_{S_{\bar{E},\Lambda}} \varphi(\vec{w}) d\nu$ for any rotation matrix $\mathcal{O}$ and any continuous function φ on the sphere $S_{\bar{E},\Lambda}$,*

then $\nu = \nu_{\bar{E},\Lambda}$, the normalized uniform measure on the sphere.

We proceed to show how the uniform measure $\nu_{\bar{E},\Lambda}$ on the constant-energy sphere $S_{\bar{E},\Lambda}$ can be realized as a mapping of a radial Gaussian measure on $\mathbb{R}^{2\Lambda}$. To this end, let

$$G_\sigma(w) = \frac{1}{\sqrt{2\pi}\sigma} e^{-\frac{w^2}{2\sigma^2}} \tag{3.20}$$

denote a Gaussian random variable with zero mean and variance σ, and let

$$G_\sigma(\vec{w}) = \prod_{j=1}^{2\Lambda} G_\sigma(w_i) \tag{3.21}$$

be the 2Λ-dimensional Gaussian distribution with the same variance. Consider the mapping $P : \mathbb{R}^{2\Lambda} \to S_{\bar{E},\Lambda}$ given by

$$\vec{w} \to \vec{y} = \sqrt{\bar{E}}\frac{\vec{w}}{|\vec{w}|} \tag{3.22}$$

with $\vec{w} \in \mathbb{R}^{2\Lambda}$, $\vec{w} \neq 0$, $P\vec{w} = \vec{y}$, and $|\vec{y}| = |P\vec{w}| = \sqrt{\bar{E}}$. Here, as in (3.6), $|\vec{w}|$ is the length of the vector $\vec{w}$. This mapping induces a probability measure ν^* on the energy sphere $S_{\bar{E},\Lambda}$ via the formula [10]

$$\int\limits_{S_{\bar{E},\Lambda}} \varphi(\vec{y}) d\nu^*(\vec{y}) = \int\limits_{\mathbb{R}^{2\Lambda}} G_\sigma(\vec{w})\varphi(P(\vec{w}))dw_1\, dw_2 \cdots dw_{2\Lambda} \tag{3.23}$$

that holds for any function φ continuous on the energy sphere $S_{\bar{E},\Lambda}$.

CLAIM 2 *The measure ν^* in* (3.23) *is precisely $\nu_{\bar{E},\Lambda}$, the normalized uniform measure on the sphere $S_{\bar{E},\Lambda}$.*

To prove this claim, we must show that the measure ν^* is invariant under rotation, that is, that it satisfies a condition analogous to (3.19). We first notice that $\mathcal{O}P\vec{w} = P\mathcal{O}\vec{w}$ for any rotation matrix $\mathcal{O}$. After the coordinate change $\vec{w} \to \mathcal{O}^{-1}\vec{w}$, we find

$$\int\limits_{S_{\bar{E},\Lambda}} \varphi(\mathcal{O}\vec{y}) d\nu^*(\vec{y}) = \int\limits_{\mathbb{R}^{2\Lambda}} G_\sigma(\mathcal{O}^{-1}\vec{w})\varphi(P(\vec{w}))dw_1\, dw_2 \cdots dw_{2\Lambda}\,.$$

Since the Gaussian distribution $G_\sigma(\vec{w})$ in (3.21) is radial, $G_\sigma(\mathcal{O}^{-1}\vec{w}g) = G_\sigma(\vec{w})$, which, together with Claim 2, concludes the proof.

By using the mapping in (3.23) and Claim 2, we can construct the following convergent Monte Carlo algorithm:

- Let $\{G_{\sigma,i}(\lambda) : i = 1, 2, \ldots, 2\Lambda\}$ be independent, identically distributed Gaussian random variables with mean zero and variance σ.
- Choose each $w_i^{(j)}$ from the distribution $G_{\sigma,i}$ at random and independently of all other $w_k^{(j)}$. Form the vector $\vec{w}^{(j)} = (w_1^{(j)}, w_2^{(j)}, \ldots, w_{2\Lambda}^{(j)})$, and let

$$\vec{y}^{(j)} = \sqrt{\bar{E}}\frac{\vec{w}^{(j)}}{|\vec{w}^{(j)}|}\,,$$

  where $|\vec{w}^{(j)}|$ is the length of the vector $\vec{w}^{(j)}$ defined as in (3.6).

Clearly, each $\vec{y}^{(j)}$ belongs to the fixed-energy sphere $S_{\bar{E},\Lambda}$.

Claims 1 and 2, and the law of large numbers [10] let us conclude the following:

CLAIM 3 *For any function φ continuous on the fixed-energy sphere $S_{\bar{E},\Lambda}$, and almost every sequence $\{\vec{y}^{(j)} : j = 1, 2, \ldots\}$, we have*

$$\lim_{M\to\infty} \frac{\sum_{j=1}^{M} \varphi(\vec{y}^{(j)})}{M} = \int\limits_{S_{\bar{E},\Lambda}} \varphi\, d\nu_{\bar{E},\Lambda}\,. \tag{3.24}$$

In other words, almost every sequence $\{\vec{y}^{(j)} : j = 1, 2, \dots\}$ generated by the above Monte Carlo algorithm is distributed uniformly over the sphere $S_{\bar{E},\Lambda}$ and can be used as a convergent quadrature procedure for calculating the integral in (3.24).

Computation of the Hamiltonian probability distribution by the Monte Carlo algorithm. Now we can use the Monte Carlo algorithm listed above to compute the probability density distribution $p_{\bar{E},\Lambda}(\lambda)$ of the Hamiltonian H in (2.26) on the sphere $S_{\bar{E},\Lambda}$ of constant energy $\bar{E}$. Here again, $\vec{w}$ is defined as in (3.3),

$$\vec{w} = (w_1, w_2, \dots, w_{2\Lambda}), \quad \hat{u}_k = w_{2k-1} + i\, w_{2k}\,, \quad k = 1, 2, \dots, \Lambda\,,$$

and $H(\vec{w})$ is computed as in (2.26),

$$H(\vec{w}) = \frac{1}{6} \sum_{\substack{k_1+k_2+k_3=0 \\ |k_1|,|k_2|,|k_3|\le\Lambda}} \hat{u}_{k_1}\hat{u}_{k_2}\hat{u}_{k_3}\,.$$

We compute the probability density $p_{\bar{E},\Lambda}(\lambda)$ via the formula

$$\int_\alpha^\beta p_{\bar{E},\Lambda}(\lambda)d\lambda = \operatorname*{Prob}_{\bar{E},\Lambda}\left\{\alpha < H(\vec{w}) < \beta\right\} = \int\limits_{S_{\bar{E},\Lambda}} \varphi\, dv_{\bar{E},\Lambda}\,, \tag{3.25}$$

where we choose the function φ to be

$$\varphi(\vec{w}) = \chi_{\{\vec{w}:\alpha<H(\vec{w})<\beta\}}(\vec{w}) \tag{3.26}$$

and

$$\chi_S(x) = \begin{cases} 1 & x \in S \\ 0 & \text{otherwise} \end{cases} \tag{3.27}$$

is the characteristic function of the set S. Equations (3.25) and (3.26), together with Claim 3, now provide the following convergent algorithm:

CLAIM 4 *From almost every sequence of vectors* $\{\vec{y}^{(j)} : j = 1, 2, \dots\}$ *generated by the Monte Carlo algorithm described on page* 18*, the probability*

$$\operatorname*{Prob}_{\bar{E},\Lambda}\left\{\alpha < Hg(\vec{w}) < \beta\right\}$$

can be computed as

$$\operatorname*{Prob}_{\bar{E},\Lambda}\left\{\alpha < H(\vec{w}) < \beta\right\} = \lim_{M\to\infty} \frac{N_{(\alpha,\beta)}}{M}\,, \tag{3.28}$$

where $N_{(\alpha,\beta)}$ *is the number of the vectors* $\vec{y}^{(j)}$, $j = 1, 2, \dots, M$, *for which the corresponding values of the Hamiltonian* H *satisfy the inequality* $\alpha < H(\vec{y}^{(j)}) < \beta$.

The Monte Carlo algorithm described above can be used to compute the probability density $p_{\bar{E},\Lambda}(\lambda)$ in (3.17) of the values of the Hamiltonian H in (2.26) on the sphere $S_{\bar{E},\Lambda}$ by "bin counting." In particular, we choose a large interval, say $[-h, h]$, within which we expect the values of the Hamiltonian H to lie. We partition it into N equal subintervals, each so small that the value of $p_{\bar{E},\Lambda}(\lambda)$ in it can be

Λ	Bin size
10	$3.5 \cdot 10^{-4}$
20	$3.0 \cdot 10^{-4}$
50	$2.0 \cdot 10^{-4}$
100	$1.5 \cdot 10^{-4}$
200	$1.0 \cdot 10^{-4}$

TABLE 3.1. Bin sizes in the bin-counting computation of the Hamiltonian probability distribution $p_{\bar{E},\Lambda}(\lambda)$ for fixed energy $E = 0.1$.

taken as approximately constant, and form an array of counters. At each computational step, we choose a point on the sphere $S_{\bar{E},\Lambda}$ by the Monte Carlo algorithm on page 18 and evaluate the Hamiltonian function (2.26) at that point. Depending on which subinterval contains the computed value of the Hamiltonian H, the value of the corresponding counter increases by 1. Each counter is then divided by the total number of the computed points and the bin size to find the approximate value of $p_{\bar{E},\Lambda}(\lambda)$ in the corresponding bin. In our computations, for each density $p_{\bar{E},\Lambda}(\lambda)$, one million, i.e., 10^6 values of the Hamiltonian H were generated via the Monte Carlo algorithm above. The standard deviation σ of the Gaussian distribution (3.21) used in the Monte Carlo algorithm was $\sigma = 1$. The number of bins in each case was 200. The sizes of the bins are presented in Table 3.1.

Probability density of the Hamiltonian. There are two natural limits to discuss as the number of degrees of freedom increases: The first one is very natural for an analogue model for geophysical applications and involves increasing Λ for fixed mean energy. This is also the natural numerical analysis limit that arises from increasing the number of Fourier modes for fixed initial data. By analogy with the ordinary extensive thermodynamic limit, the behavior as Λ increases while the energy per mode is held constant is also interesting. Here we report the results for the first situation, but the interested reader can consult Abramov's doctoral thesis [2] for the second situation.

Here we present the results of Monte Carlo simulations for the densities $p_{\bar{E},\Lambda}(\lambda)$ for a fixed mean energy $\bar{E}$ as Λ increases, i.e., $\bar{E} = 0.1$, and $\Lambda = 10, 20, 50, 100, 200$.

Self-similar scaling at fixed total energy. For the case of fixed energy, $E = \bar{E} = 0.1$, we display the computed probability densities $p_{\bar{E},\Lambda}(\lambda)$ in Figures 3.1 and 3.2.

We observe that these probability measures are Gaussian-like, and while they are not Gaussian, they have an approximately self-similar form, that is,

$$p_{\bar{E},\Lambda}(\lambda) = \sigma_H(\Lambda) p_{\bar{E}}\left(\frac{\lambda}{\sigma_H(\Lambda)}\right). \tag{3.29}$$

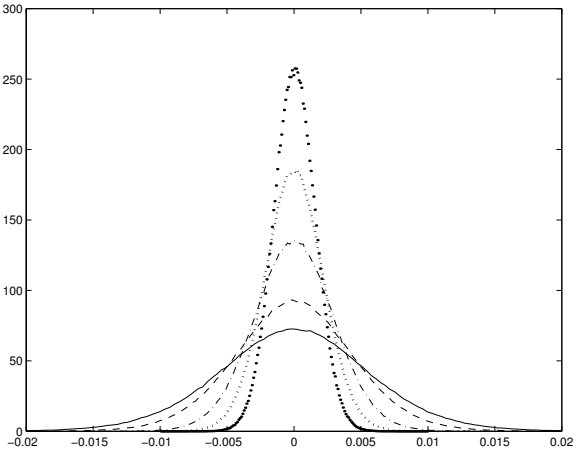

FIGURE 3.1. PDFs $p_{\bar{E}}(\Lambda)$ of the Hamiltonian at fixed energy $E = 0.1$. Solid line: $\Lambda = 10$; dashed line: $\Lambda = 20$; dash-dotted line: $\Lambda = 50$; dotted line: $\Lambda = 100$; dots: $\Lambda = 200$.

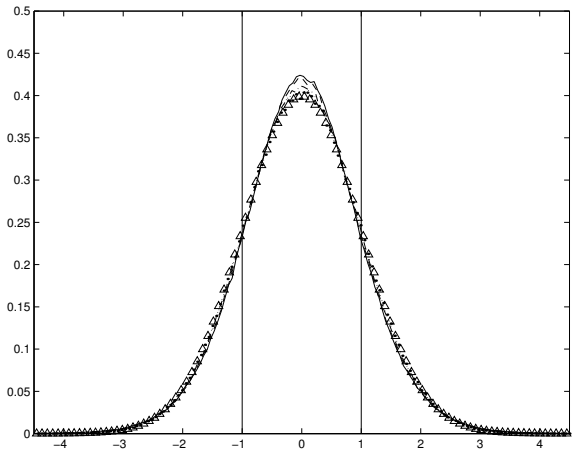

FIGURE 3.2. Rescaled PDFs $p_{\bar{E}}(\Lambda)$ of the Hamiltonian at fixed energy $E = 0.1$: self-similarity. Solid line: $\Lambda = 10$; dashed line: $\Lambda = 20$; dash-dotted line: $\Lambda = 50$; dotted line: $\Lambda = 100$; dots: $\Lambda = 200$; triangles: Gaussian fit $\sigma = 1$; vertical lines denote standard deviation.

Here

$$\sigma_H(\Lambda) = \sqrt{\int_{-\infty}^{\infty} \lambda^2 p_{\bar{E},\Lambda}(\lambda) d\lambda} \tag{3.30}$$

$E = 0.1$, flatness		$E = 0.1$, dependence $\sigma_H(\Lambda)$	
Λ	M_4/M_2^2	Λ	$\sigma_H(\Lambda)$
10	3.5130	10	$6.2 \cdot 10^{-3}$
20	3.4518	20	$4.7 \cdot 10^{-3}$
50	3.2646	50	$3.2 \cdot 10^{-3}$
100	3.1466	100	$2.4 \cdot 10^{-3}$
200	3.0732	200	$1.8 \cdot 10^{-3}$

TABLE 3.2. On the left, the flatness (ratio between the fourth moment and squared second moment) of PDFs, $p_{\bar{E},\Lambda}(\lambda)$, of the Hamiltonian for different values of $\bar{E}$ and Λ. On the right, the dependence of $\sigma_H(\Lambda)$ on Λ for fixed energy, $E = 0.1$.

is the width of the distribution $p_{\bar{E},\Lambda}(\lambda)$, and $p_{\bar{E}}(\lambda)$ is a symmetric probability distribution that is slightly super-Gaussian; that is, it has flatness

$$\frac{M_4}{M_2^2} = \frac{\int_{-\infty}^{\infty} \lambda^4 p_{\bar{E},\Lambda}(\lambda) d\lambda}{(\int_{-\infty}^{\infty} \lambda^2 p_{\bar{E},\Lambda}(\lambda) d\lambda)^2} > 3\,.$$

In particular, the flatness of $p_{\bar{E}}(\lambda)$ is represented in Table 3.2. The values of the width $\sigma_H(\Lambda)$ as a function of the truncation size Λ are also presented in Table 3.2. Data from Table 3.2 are used to rescale the distributions $p_{\bar{E},\Lambda}(\lambda)$ and confirm the self-similar scaling form (3.29). The results are shown in Figure 3.2.

After plotting $\sigma_H(\Lambda)$ versus Λ and $\log(\sigma_H(\Lambda))$ versus $\log(\Lambda)$ with a remarkable straight-line fit in Figure 3.3, we see that the results presented in Table 3.2 furnish powerful numerical evidence that the width $\sigma_H(\Lambda)$ scales with the truncation size Λ according to the formula

$$\sigma_H(\Lambda) = A_0 \Lambda^{\alpha}\,, \quad \alpha = -0.413899 \pm 8.98 \cdot 10^{-4}\,, \tag{3.31}$$

where A_0 was determined to be $A_0 = 1.615 \cdot 10^{-2}$. The systematic decrease of the flatness in Table 3.2 to the Gaussian value 3 as Λ increases, as well as the essentially Gaussian rescaled PDFs in Figure 3.2, clearly suggests that the Hamiltonian obeys a central limit theorem. In the fixed energy per mode case, $\sigma_H(\Lambda)$ scales linearly with Λ (see [2]), which is indicative of a more straightforward central limit theorem behavior in the thermodynamic limit.

Mixed canonical-microcanonical distribution in the large Λ limit at fixed energy. In order to understand why the Hamiltonian is largely a statistically irrelevant conserved quantity in the large Λ limit at fixed energy E, here we consider statistical ensembles of solutions of the truncated Burgers-Hopf equation (2.27), distributed according to the mixed canonical-microcanonical distribution (3.16), and show that the values of the Hamiltonian H are expected to be very close to zero in this limit.

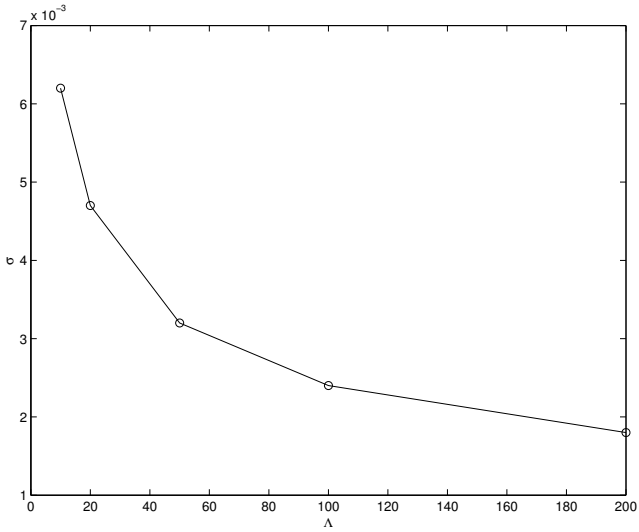

Plot of σ_H vs. Λ.

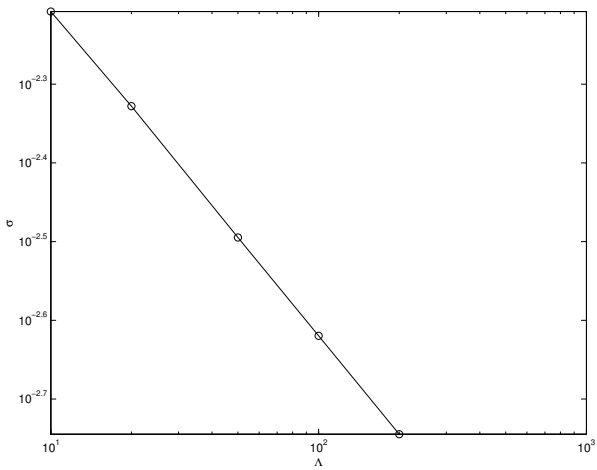

Plot of $\log(\sigma_H)$ vs. $\log(\Lambda)$.

FIGURE 3.3. $\sigma_H(\Lambda)$ versus Λ and $\log(\sigma_H)$ versus $\log(\Lambda)$, $E = 0.1$. On the second plot we see the power law $\sigma_H(\Lambda) = A_0\Lambda^\alpha$.

We exploit the empirical self-similar scaling law verified in the last section and a simple small-deviation argument to establish this. Our numerical results of direct simulation, presented in Section 4, show that, in the near-zero regime, the Hamiltonian is indeed irrelevant.

The key feature that we need to understand is how the Hamiltonian scales on average in the limit as the truncation size Λ increases, $\Lambda \to \infty$, with the energy $\bar{E}$ fixed. We begin by computing the average value of the Hamiltonian from (3.16)

with respect to such a measure as

$$\bar{H} = \frac{\int_{S_{\bar{E},\Lambda}} H(u) e^{-\theta H(u)}\, dv_{\bar{E},\Lambda}}{\int_{S_{\bar{E},\Lambda}} e^{-\theta H(u)}\, dv_{\bar{E},\Lambda}}\,. \tag{3.32}$$

With the probability density $p_{\bar{E},\Lambda}(\lambda)$, we have

$$\bar{H} = \frac{\int_{-\infty}^{\infty} \lambda e^{-\theta\lambda} p_{\bar{E},\Lambda}(\lambda) d\lambda}{\int_{-\infty}^{\infty} e^{-\theta\lambda} p_{\bar{E},\Lambda}(\lambda) d\lambda}\,, \tag{3.33}$$

and by combining the empirical equation in (3.29) with (3.33) and rescaling $\lambda \to \sigma_H(\Lambda)\,\lambda$, we conclude

$$\bar{H}(\theta) = \frac{\sigma_H(\Lambda) \int_{-\infty}^{\infty} \lambda e^{-\sigma_H(\Lambda)\theta\lambda} p_{\bar{E}}(\lambda) d\lambda}{\int_{-\infty}^{\infty} e^{-\sigma_H(\Lambda)\theta\lambda} p_{\bar{E}}(\lambda) d\lambda}\,. \tag{3.34}$$

Thus, for any fixed θ, due to (3.31), Taylor-expanding (3.34) yields

$$\lim_{\Lambda\to\infty} \frac{\bar{H}(\theta)}{\sigma_H(\Lambda)} = -\int_{-\infty}^{\infty} \lambda^2 p_{\bar{E}}(\lambda) d\lambda\,, \tag{3.35}$$

that is,

$$\bar{H}(\theta) = -\sigma_H(\Lambda)^2 \theta \bar{\sigma}^2 + o(\sigma_H(\Lambda))^2 \quad \text{where } \bar{\sigma}^2 = \int_{-\infty}^{\infty} \lambda^2 p_{\bar{E}}(\lambda) d\lambda\,. \tag{3.36}$$

In particular, statistical values of the Hamiltonian H indeed concentrate very sharply near zero for a fixed inverse temperature θ, that is,

$$\left|\bar{H}(\theta)\right| = O\left(\sigma_H(\Lambda)^2 \bar{\sigma}^2\right) \ll 1\,. \tag{3.37}$$

In other words, for a fixed inverse temperature θ and energy $\bar{E}$ and in the limit as $\Lambda \to \infty$, the expected values of the Hamiltonian H in a mixed microcanonical energy and canonical Hamiltonian ensemble are typical values of the distribution (3.16), and thus, according to our computational results presented in Section 4, irrelevant for the statistical mechanics of the Burgers-Hopf equations (2.27).

Statistically relevant and irrelevant values of the Hamiltonian. We now give precise definitions of the terms *relevant* and *irrelevant* values of the Hamiltonian H in (2.26) for the statistical mechanics of the truncated Burgers-Hopf equations (2.27).

- An *irrelevant* value of the Hamiltonian H means the existence of
  - an equipartition spectrum (3.9) and
  - essentially universal correlation structure.
- A *relevant* value of the Hamiltonian H means
  - a significant tilt to the spectrum and
  - longer tails of the correlation functions on large-scale modes.

Our computations, described in the forthcoming sections, show that relevant and irrelevant values of the Hamiltonian can be identified in terms of its probability distribution function $p_{\bar{E},\Lambda}(\lambda)$. We have seen in the previous sections that the probability distribution function $p_{\bar{E},\Lambda}(\lambda)$ of the Hamiltonian H in (2.26), generated by the above-described Monte Carlo simulation, possesses two key properties:

(1) $p_{\bar{E},\Lambda}(\lambda)$ is a symmetric probability distribution about zero, and, for fixed energy $\bar{E}$, $p_{\bar{E},\Lambda}(\lambda)$ has an increasingly small variance as $\Lambda \to \infty$.
(2) $p_{\bar{E},\Lambda}(\lambda)$ is approximately self-similar according to the formula (3.29),

$$p_{\bar{E},\Lambda}(\lambda) = \sigma_H(\Lambda)\ p_{\bar{E}}\left(\frac{\lambda}{\sigma_H(\Lambda)}\right) \quad \text{with } \sigma_H(\Lambda) \to 0 \text{ as } \Lambda \to \infty.$$

Property 1 yields, for fixed $\bar{E}$ and $\Lambda \to \infty$, the concentration of the probability density $p_{\bar{E},\Lambda}(\lambda)$ of the Hamiltonian H near the hypersurface $H(u) = 0$. Property 2 allows us to access the rare events of the distribution.

The Monte-Carlo-generated equilibrium probability distribution $p_{\bar{E},\Lambda}(\lambda)$ leads to the following classification:

- *Typical* values of the Hamiltonian H are the ones within the standard deviation $\sigma_H(\Lambda)$.
- *Atypical* values of the Hamiltonian H are, in absolute value, larger than $\sigma_H(\Lambda)$ and occupy a set of vanishingly small measure as Λ increases for any fixed mixed canonical-microcanonical Gibbs measure according to (3.37). Recall from (3.37) that the mean value of H scales like σ_H^2.

In the rest of the paper we present strong numerical evidence that the typical values of the Hamiltonian are statistically irrelevant in the sense described above.

3.3 The Numerical Algorithm and a Basic Simulation

All the numerical data presented in this paper were obtained by utilizing a standard numerical method to compute the solutions of the truncated Burgers-Hopf equation (2.14). The method solves the truncated Burgers-Hopf equation (2.14) pseudospectrally in de-aliased form. In particular, the fast Fourier transform procedure, $\mathrm{FFT}\{[\mathrm{FFT}^{-1}(u_\Lambda)]^2\}$, is used to compute the nonlinear term. For this algorithm we use an expanded array of $2(2\Lambda + 1) + 1$ Fourier terms, setting all but the ones with indices $|k| \leq \Lambda$ equal to zero in order to avoid aliasing. This method calls for only $\mathcal{O}(\Lambda \log(\Lambda))$ floating point operations. We use the sixth-order Adams-Bashforth linear multistep method [5] for the time stepping. With the time step 0.001, this algorithm conserves the energy (2.29) within $10^{-8}\%$ and the Hamiltonian (2.26) within $10^{-9}\%$ for all simulations presented in this paper.

Besides the mean energy per mode in (3.9), the correlation functions (3.10), and the correlation times (3.11), in this paper we also employ as diagnostic tools

the probability distribution functions of each mode (PDFs), given by the formulae

$$\begin{aligned} \text{Prob}\left\{\alpha < \text{Re}(\hat{u}_k) < \beta\right\} &= \int_\alpha^\beta \rho_{\text{Re}(\hat{u}_k)}(\lambda) d\lambda \,, \\ \text{Prob}\left\{\alpha < \text{Im}(\hat{u}_k) < \beta\right\} &= \int_\alpha^\beta \rho_{\text{Im}(\hat{u}_k)}(\lambda) d\lambda \,. \end{aligned} \tag{3.38}$$

In order to compute the PDFs, we again use "bin counting." In particular, in our computations, we follow the modes $\hat{u}_k(t)$, $k = 1, 2, \ldots, \Lambda$, for $T_0 < t < T_0 + T$, where T_0 is the initial time and T is the length of the averaging window. (In most of the computations, $T_0 = 1000$ and $T = 20000$.) We choose an interval, say $[-L, L]$, in which we expect the random values of $\text{Re}(\hat{u}_k(t))$ and $\text{Im}(\hat{u}_k(t))$ to be distributed, and partition it into N equal subintervals. For each $\text{Re}(\hat{u}_k(t))$ or $\text{Im}(\hat{u}_k(t))$, we then form an array of N counters, each of whose values increases by 1 at the n^{th} time step (of size Δt) if the value of the current random variable $\text{Re}(\hat{u}_k(T_0 + n\Delta t))$ or $\text{Im}(\hat{u}_k(T_0 + n\Delta t))$ is contained in the corresponding subinterval. Finally, we divide each element of the array of counters by the total number of time steps and multiply it by $N/2L$, so that the distribution is normalized on the interval $[-L, L]$. For all the computational results in this paper, we have displayed the PDFs of the imaginary parts of the modes, $\text{Im}(\hat{u}_k(T_0 + n\Delta t))$. The sizes and numbers of bins are shown with the results of each computation.

Here we present a prototypical simulation where $H = 0$, which is clearly the most irrelevant value of the Hamiltonian for the equilibrium statistical mechanics of the truncated Burgers-Hopf equations (2.27). For this simulation, the truncation size is $\Lambda = 50$, and the initial condition is $u_\Lambda(x, 0) = \sin x + 0.5 \cos 4x$. This initial condition indeed satisfies the equation $H = 0$. It also has no special symmetry; that is, it is neither an odd nor an even function nor a spatial shift of one. We use the pseudospectral method to compute the corresponding solution. The time step is $\Delta t = 10^{-3}$, the initial averaging time is $T_0 = 1000$, and the averaging window $T = 20000$. The energy in (2.29) and the Hamiltonian in (2.26) are conserved within $10^{-8}\%$ and $10^{-9}\%$, respectively. The number of bins in the bin-counting procedure was 200, and the size of each bin was $1.5 \cdot 10^{-2}$. As expected, the energy spectrum in Figure 3.4 is completely flat and in excellent agreement with the analytical prediction (3.9). The PDFs for representative modes $k = 1$ and $k = 20$ in Figure 3.5 are indistinguishable from the Gaussians predicted from the analytical energy-based Gibbs formula (3.5). The computed correlation functions for modes $k > 1$ exhibit almost no oscillations, and the corresponding correlation times agree almost perfectly with the analytical scaling prediction (3.12). In order to condense the number of figures in the paper, we refer the reader to the corresponding figures in [12], since our results are identical to the ones presented there. However, the PDF results in Figure 3.5 are new.

The original work of [12, 13] on the truncated Burgers-Hopf equation (2.27) employed the pseudospectral method together with a host of initial conditions to study statistical properties of this equation. The deterministic initial conditions

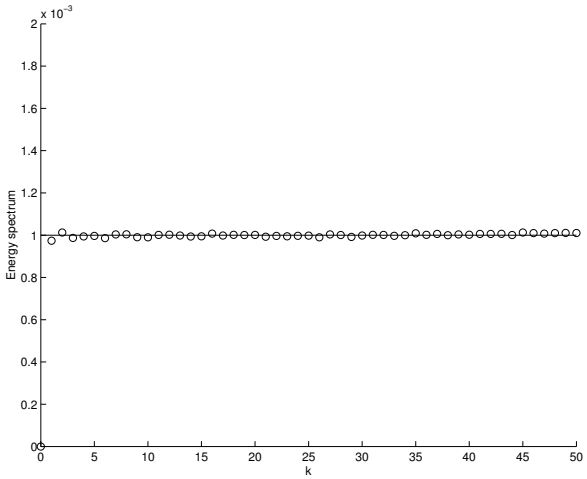

FIGURE 3.4. Energy spectrum for $\sin(x) + 0.5\cos(4x)$ with $H = 0$, $\Lambda = 50$, $E = 0.1$. Circles: numerical simulation with $H = 0$; horizontal line implies equipartitioned spectrum.

were either small perturbations of initial data generating exact solutions with subharmonic instability [13] or the classical data $2\sin(x)$ [12]. The Hamiltonian vanishes identically for these deterministic initial data. In the cases with random initial data [13], the procedure utilized to select the initial data automatically guarantees statistically irrelevant values for the Hamiltonian in the precise sense in the previous section. All types of initial conditions led to the robust statistical behavior also observed in our simulation described in the previous paragraph, namely, energy equipartition (3.7) and correlation time scaling proportional to the eddy turnover time (3.12).

Paradoxically, one of the authors in his doctoral thesis [2] developed simulations of (2.27) using direct summation to compute the nonlinear term and the initial condition $2\sin(x)$ that do not lead to robust statistical behavior. In particular, computations in [2] indicate that odd initial data such as $2\sin(x)$ often lie on a large homoclinic manifold that can be tracked by the direct summation method for far longer times than by the pseudospectral method due to different roundoff errors incurred by each method. When the pseudospectral method is used, roundoff error pushes the solution off of this homoclinic manifold within a moderate amount of time, thus recovering the statistically robust regime. Extensive details documenting this behavior can be found in [2] and will be published elsewhere.

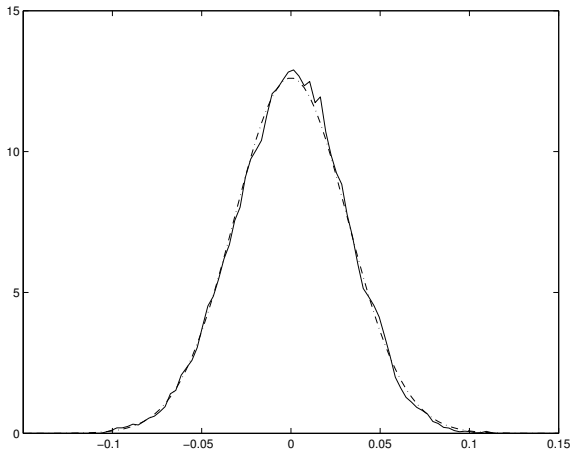

Mode $k = 1$.

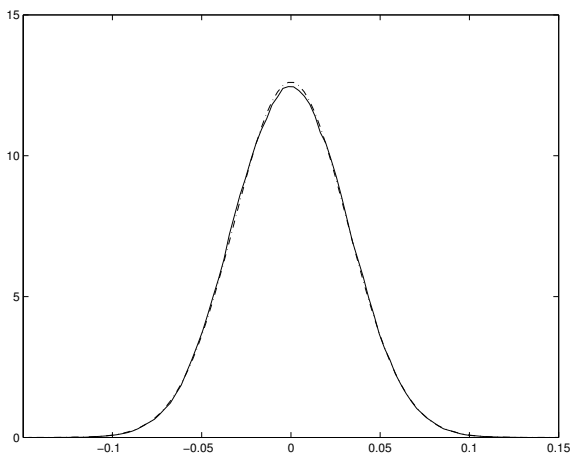

Mode $k = 20$.

FIGURE 3.5. PDFs for $\sin(x) + 0.5\cos(4x)$ with $H = 0$, $\Lambda = 50$, $E = 0.1$. Solid line: numerical result; dashed line: Gaussian with the same variance.

4 When Is the Hamiltonian a Statistically Irrelevant Conserved Quantity? A Numerical Study

In this section, we present powerful numerical evidence utilizing the numerical procedure in Section 3.3 of the role of the Hamiltonian H in (2.26) for the equilibrium statistical mechanics of the truncated Burgers-Hopf equations as described in Sections 3.1 and 3.2. The experiments confirm the precise quantitative guidelines for statistically relevant and irrelevant values of the Hamiltonian developed at the end of Section 3.2. In particular, our simulations furnish powerful numerical evidence that typical values of the Hamiltonian are irrelevant in the sense that

they do not significantly affect the energy equipartition in (3.9) and that the corresponding correlation functions exhibit little oscillation, while atypical values of the Hamiltonian are relevant in the sense that they produce a significant spectral tilt and slower decay with large oscillations in the correlation functions.

In the results reported below we have used both the deterministic initial condition

$$u_\Lambda(x,0) = \sqrt{2E}(\sin x + \cos 2x)\,, \tag{4.1}$$

which is not a shift of an odd function, as well as random initial conditions generated by one step of the Monte Carlo procedure on page 18. In the initial conditions (4.1), the multiplicative constant is chosen so that the initial condition and the subsequent solution satisfy the predetermined value of the energy E in (2.29).

As in [12, 13], in all our calculations with the deterministic initial data (4.1), we observe that the solution passes through three stages of randomization. The first stage is the deterministic stage before shocks develop in the corresponding untruncated Burgers-Hopf solution, the second the stage shortly after the breaking time when ripples appear on top of the still-deterministic solution, and the third the completely randomized stage. These stages are shown in figure 1 of [12] and are not repeated here.

We present the case with the energy fixed at $E = 0.1$ and increasing truncation sizes $\Lambda = 10, 20, 50, 100, 200$. The pseudospectral method was used in the computations, the time step was $\Delta t = 10^{-3}$, the initial averaging time was $T_0 = 1000$, and the averaging window was $T = 20000$. Two sets of simulations with random initial conditions are presented. One set of deterministic initial conditions (4.1) is also presented for $\Lambda = 20$ and $\Lambda = 50$. Table 3.2 shows the widths $\sigma_H(\Lambda)$ of the Hamiltonian probability distribution functions $p_{\bar{E},\Lambda}(\lambda)$ for these values of Λ. For the deterministic initial data (4.1), the value of the Hamiltonian function is $H = -1.1 \cdot 10^{-2}$, which is never a typical value, since Table 3.2 shows that its magnitude always exceeds the standard deviation $\sigma_H(\Lambda)$. In all the computations, the energy in (2.29) and the Hamiltonian in (2.26) were conserved within $10^{-8}\%$ and $10^{-9}\%$, respectively. The number of bins in the bin-counting procedure for constructing the PDFs of the modes is 200 in all cases. The sizes of the bins are shown in Table 4.1.

The numerical results presented below give clear evidence that for atypical values of the Hamiltonian, the energy spectra are tilted compared to the equipartition prediction (3.9). We display the sizes of the tilts in Table 4.2, for which we assume the linear fit $E_k = a_0 + a_1 k$ and record the values of the coefficient a_1. Moreover, in Table 4.3, we provide the L_2 errors between the numerically computed PDFs and the predicted analytical Gaussian from the energy-based Gibbs distribution (3.5).

For $\Lambda = 10$ and random initial data, the values of the Hamiltonian H are $H = 10^{-2}$ and $H = -1.9 \cdot 10^{-3}$, respectively. The former is highly atypical, and the latter is typical. This is confirmed by the energy spectra in Figure 4.1 and the recorded tilts in Table 4.2, where the spectrum corresponding to $H = 10^{-2}$ is

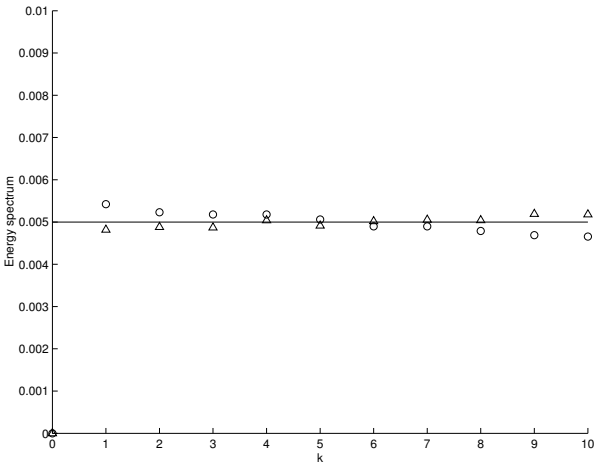

(a) Energy spectrum. Circles: $H = 10^{-2}$; triangles: $H = -1.9 \cdot 10^{-3}$; horizontal line implies equipartitioned spectrum.

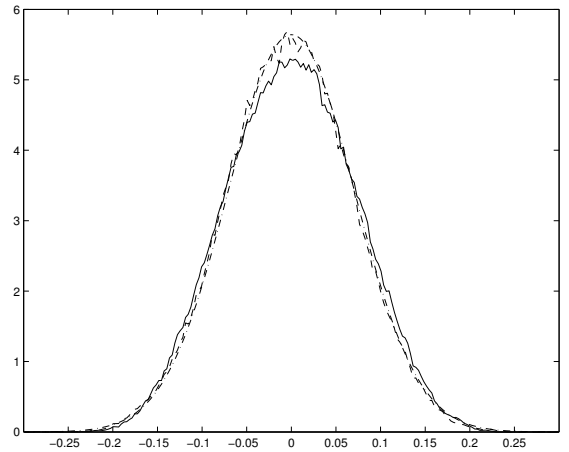

(b) PDF for mode $k = 1$. Solid line: $H = 10^{-2}$; dashed line: $H = -1.9 \cdot 10^{-3}$; dash-dotted line: Gaussian fit with the same variance centered at zero.

FIGURE 4.1. (a) Energy spectrum and (b) PDF for random initial data, $\Lambda = 10$, $E = 0.1$.

considerably more tilted. The average PDF over all modes is also less Gaussian in the atypical case according to Table 4.3. The correlation function for the $H = 10^{-2}$ case also exhibits considerably larger oscillations than the correlation function for the $H = -1.9 \cdot 10^{-3}$ case. The correlation functions for the $k = 1$ mode are shown in Figure 4.2. For both cases the correlation times obey the formula for the scaling law in (3.12) quite accurately, as is also shown in Figure 4.2.

Λ	Bin size
10	$3.0 \cdot 10^{-3}$
20	$3.0 \cdot 10^{-3}$
50	$1.5 \cdot 10^{-3}$
100	$1.5 \cdot 10^{-3}$
200	$1.0 \cdot 10^{-3}$

TABLE 4.1. Bin sizes in the bin-counting computation of the PDFs of the modes for fixed energy $E = 0.1$.

$\Lambda = 10$, $H = 10^{-2}$	$a_1 = -8.279 \cdot 10^{-5}$
$\Lambda = 10$, $H = -1.9 \cdot 10^{-3}$	$a_1 = 3.895 \cdot 10^{-5}$
$\Lambda = 20$, $H = -4.7 \cdot 10^{-3}$	$a_1 = 5.797 \cdot 10^{-7}$
$\Lambda = 20$, $H = -1.9 \cdot 10^{-3}$	$a_1 = 3.266 \cdot 10^{-6}$
$\Lambda = 20$, $H = -1.1 \cdot 10^{-2}$	$a_1 = -2.693 \cdot 10^{-5}$
$\Lambda = 50$, $H = 8 \cdot 10^{-3}$	$a_1 = -1.982 \cdot 10^{-6}$
$\Lambda = 50$, $H = 2 \cdot 10^{-3}$	$a_1 = 1.543 \cdot 10^{-7}$
$\Lambda = 50$, $H = -1.1 \cdot 10^{-2}$	$a_1 = -3.603 \cdot 10^{-6}$
$\Lambda = 100$, $H = -1.1 \cdot 10^{-3}$	$a_1 = 2.843 \cdot 10^{-8}$
$\Lambda = 100$, $H = -2.2 \cdot 10^{-3}$	$a_1 = 1.018 \cdot 10^{-8}$
$\Lambda = 200$, $H = -6.3 \cdot 10^{-4}$	$a_1 = 2.843 \cdot 10^{-8}$
$\Lambda = 200$, $H = 3.8 \cdot 10^{-5}$	$a_1 = 1.018 \cdot 10^{-8}$

TABLE 4.2. Tilt in the energy spectra. Results are fitted with $E_k = a_0 + a_1 k$ at fixed energy $E = 0.1$.

$\Lambda = 10$, $H = 10^{-2}$	$L_{\text{err}} = 1.59 \cdot 10^{-1}$
$\Lambda = 10$, $H = -1.9 \cdot 10^{-3}$	$L_{\text{err}} = 9.29 \cdot 10^{-2}$
$\Lambda = 20$, $H = -4.7 \cdot 10^{-3}$	$L_{\text{err}} = 1.01 \cdot 10^{-1}$
$\Lambda = 20$, $H = -1.9 \cdot 10^{-3}$	$L_{\text{err}} = 1.54 \cdot 10^{-1}$
$\Lambda = 20$, $H = -1.1 \cdot 10^{-2}$	$L_{\text{err}} = 2.18 \cdot 10^{-1}$
$\Lambda = 50$, $H = 8 \cdot 10^{-3}$	$L_{\text{err}} = 1.12 \cdot 10^{-1}$
$\Lambda = 50$, $H = 2 \cdot 10^{-3}$	$L_{\text{err}} = 1.11 \cdot 10^{-1}$
$\Lambda = 50$, $H = -1.1 \cdot 10^{-2}$	$L_{\text{err}} = 3.26 \cdot 10^{-1}$
$\Lambda = 100$, $H = -1.1 \cdot 10^{-3}$	$L_{\text{err}} = 1.29 \cdot 10^{-1}$
$\Lambda = 100$, $H = -2.2 \cdot 10^{-3}$	$L_{\text{err}} = 1.11 \cdot 10^{-1}$
$\Lambda = 200$, $H = -6.3 \cdot 10^{-4}$	$L_{\text{err}} = 1.70 \cdot 10^{-1}$
$\Lambda = 200$, $H = 3.8 \cdot 10^{-5}$	$L_{\text{err}} = 1.48 \cdot 10^{-1}$

TABLE 4.3. L_2 error between numerically obtained PDFs and their Gaussian analytical fits at fixed energy $E = 0.1$.

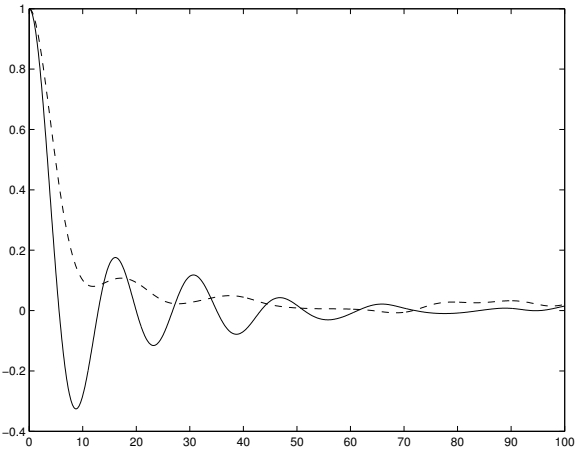

(a) Time correlations for random initial data, mode $k = 1$. Solid line: $H = 10^{-2}$; dashed line: $H = -1.9 \cdot 10^{-3}$.

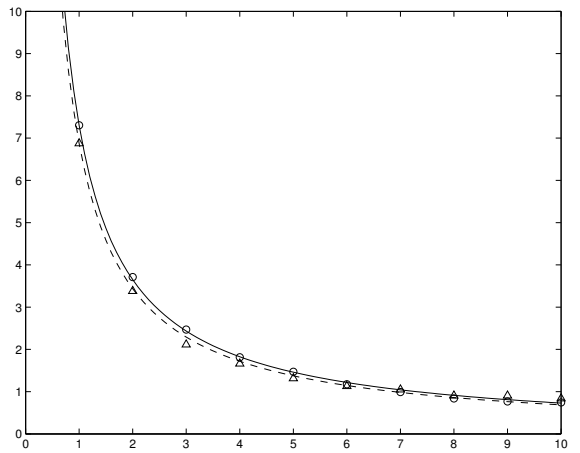

(b) Correlation times. Circles: $H = 10^{-2}$; triangles: $H = -1.9 \cdot 10^{-3}$; solid line: fit $C\sqrt{\beta}/k$ for circles, $C = 0.7303$; dashed line: fit $C\sqrt{\beta}/k$ for triangles, $C = 0.6875$.

FIGURE 4.2. (a) Correlation function and (b) correlation time scaling for $\Lambda = 10$, $E = 0.1$.

For $\Lambda = 20$, both values of the Hamiltonian H for random initial data, $H = -4.7 \cdot 10^{-3}$ and $H = -2.2 \cdot 10^{-3}$, are typical. As shown in Figure 4.3 and Tables 4.2 and 4.3, their energy spectra and PDFs agree very well with the theoretical predictions (3.9) and the Gaussian form implied by (3.5), respectively. The energy spectrum of the solution with the deterministic initial data (4.1) is considerably more tilted, and the PDF is farther away from the Gaussian; see Tables 4.2 and 4.3. Although the correlation functions for the solutions corresponding to the two sets of random initial data are close to one another and exhibit only small oscillations,

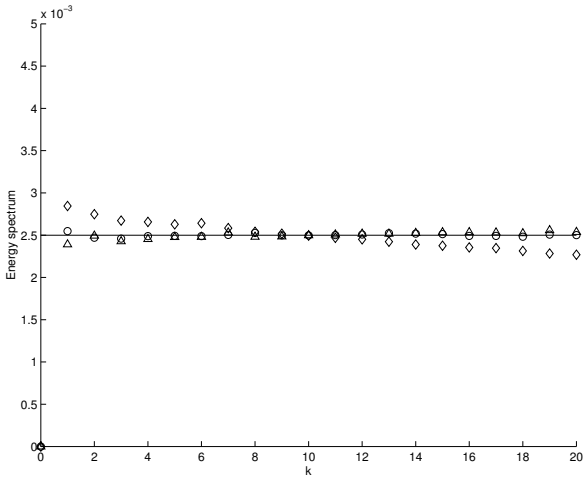

(a) Energy spectrum. Circles: $H = -4.7 \cdot 10^{-3}$; triangles: $H = -2.2 \cdot 10^{-3}$; diamonds: $H = -1.1 \cdot 10^{-2}$; horizontal line implies equipartitioned spectrum.

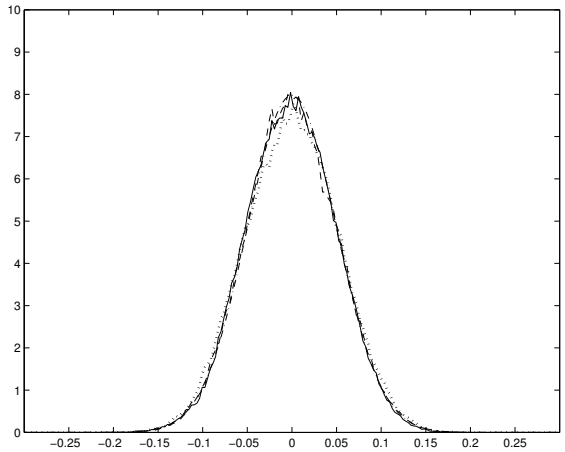

(b) PDF, mode $k = 1$. Solid line: $H = -4.7 \cdot 10^{-3}$; dashed line: $H = -2.2 \cdot 10^{-3}$; dotted line: $H = -1.1 \cdot 10^{-2}$; dash-dotted line: Gaussian fit with the same variance centered at zero.

FIGURE 4.3. (a) Energy spectrum and (b) PDF for random and deterministic initial data, $\Lambda = 20$, $E = 0.1$.

the correlation function for the solutions corresponding to the deterministic initial data oscillates more strongly, as shown in Figure 4.4. Both sets of data produce a reasonably good fit with the correlation scaling law (3.12), as shown in Figure 4.5.

For $\Lambda = 50$, random initial data yield the values of the Hamiltonian $H = 8 \cdot 10^{-3}$ and $H = 2 \cdot 10^{-3}$, respectively. The former is atypical, and the latter is typical. This is reflected in the tilts of the energy spectra in Figure 4.6 and Table 4.2, and,

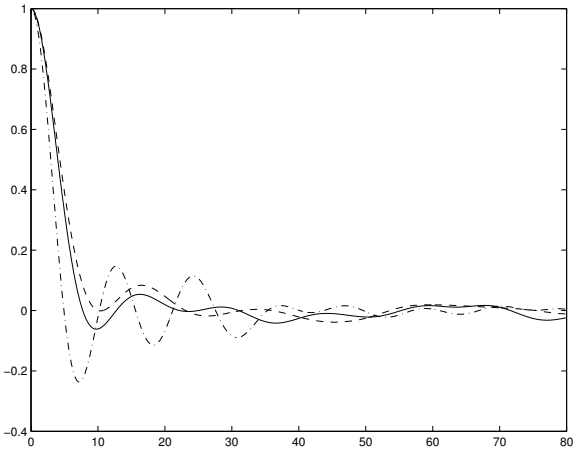

FIGURE 4.4. Time correlations for random and deterministic initial data, $\Lambda = 20$, $E = 0.1$, mode $k = 1$. Solid line: $H = -4.7 \cdot 10^{-3}$; dashed line: $H = -2.2 \cdot 10^{-3}$; dash-dotted line: $H = -1.1 \cdot 10^{-2}$.

to a lesser extent, the oscillations of the correlation functions. The PDFs are close to Gaussian; see Table 4.3. The tilt for the deterministic initial data is considerably larger, since the corresponding value of the Hamiltonian, $H = -1.1 \cdot 10^{-2}$, is highly atypical, and the PDF is much farther away from the Gaussian than the PDF for random initial data, as shown in Figure 4.6 and Tables 4.2 and 4.3. Correlation scaling formula (3.12) is a good fit in all three cases, as seen in Figure 4.7.

For $\Lambda = 100$, the values of the Hamiltonian along the solutions generated by the random initial data are $H = -1.1 \cdot 10^{-3}$ and $H = -2.2 \cdot 10^{-3}$, respectively. Both of these values are typical. The energy spectra and the PDFs are almost indistinguishable from their theoretically predicted counterparts, as shown in Figure 4.8 and Tables 4.2 and 4.3. Except for $k = 1$, the correlation functions are also indistinguishable. The fit of the correlation times with the scaling formula (3.12) is excellent, as shown in Figure 4.10.

For $\Lambda = 200$, the values of the Hamiltonian corresponding to the two randomly generated sets of initial data are $H = -6.3 \cdot 10^{-4}$ and $H = 3.8 \cdot 10^{-5}$, respectively, which are both typical. They give excellent agreement with the theoretical predictions, as shown in Figures 4.9 and 4.10 and Tables 4.2 and 4.3. These last two cases confirm the robustness of the predictions of the statistical theory based solely on the Gibbs measure for energy [12, 13].

The results of this section thus furnish strong numerical evidence to support the prediction of Section 3.2 that typical values of the Hamiltonian H in (2.26) are irrelevant for the statistical mechanics of the Burgers-Hopf equations in (2.27). This is reflected in the fact that the corresponding solutions exhibit negligible spectral tilts, essentially universal structure of the correlation functions with very small oscillations, and PDFs close to Gaussian. On the other hand, we have also provided

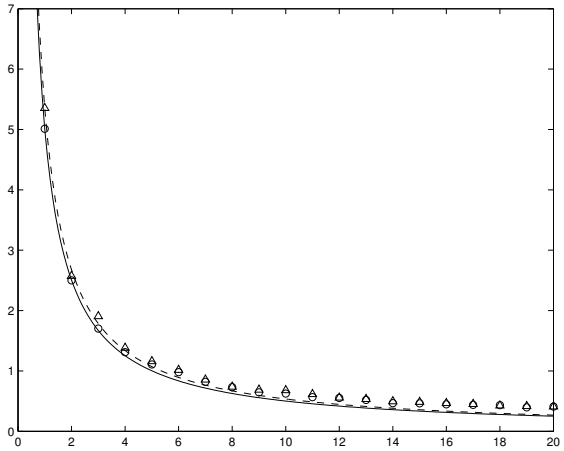

(a) Random initial data. Circles: $H = -4.7 \cdot 10^{-3}$; triangles: $H = -2.2 \cdot 10^{-3}$; solid line: fit $C\sqrt{\beta}/k$ for circles, $C = 0.3544$; dashed line: fit $C\sqrt{\beta}/k$ for triangles, $C = 0.3786$.

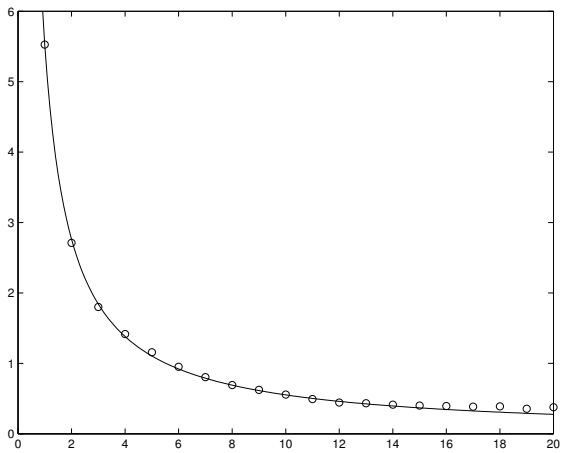

(b) $\sin(x) + \cos(2x)$ initial data. Circles: $H = 1.1 \cdot 10^{-2}$; solid line: fit $C\sqrt{\beta}/k$, $C = 0.3908$.

FIGURE 4.5. Correlation time scaling for (a) random and (b) deterministic initial data, $\Lambda = 20$, $E = 0.1$.

strong numerical evidence that atypical values of the Hamiltonian are relevant in the sense that the corresponding solutions exhibit considerable spectral tilts, strong oscillations of the correlation functions, and PDFs farther away from Gaussian. However, the correlation scaling law is also valid for the atypical cases. Numerical simulations in the situation with fixed energy per mode are reported in [2] and will be presented elsewhere. In this limit, the tilt in the energy spectrum is less noticeable as Λ increases.

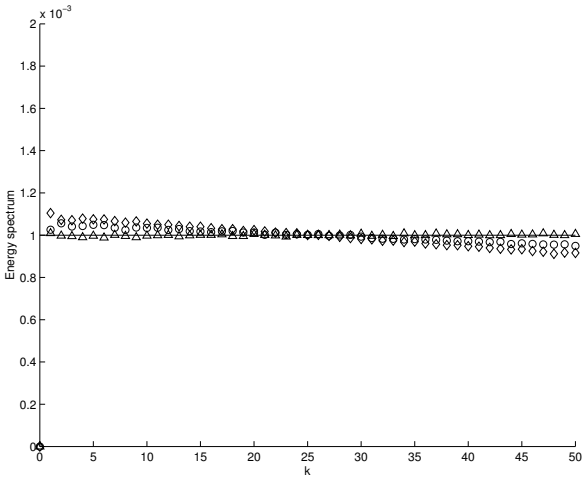

(a) Energy spectrum. Circles: $H = 8 \cdot 10^{-3}$; triangles: $H = 2 \cdot 10^{-3}$; diamonds: $H = -1.1 \cdot 10^{-2}$; horizontal line implies equipartitioned spectrum.

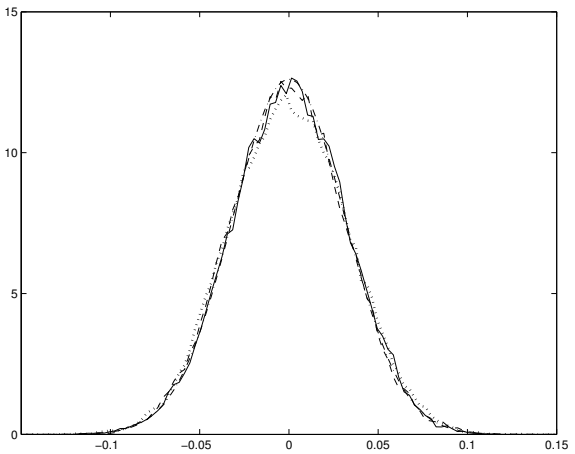

(b) PDF for mode $k = 1$. Solid line: $H = 8 \cdot 10^{-3}$; dashed line: $H = 2 \cdot 10^{-3}$; dotted line: $H = -1.1 \cdot 10^{-2}$; dash-dotted line: Gaussian fit with the same variance centered at zero.

FIGURE 4.6. (a) Energy spectrum and (b) PDF for random initial data, $\Lambda = 50$, $E = 0.1$.

5 Equilibrium Statistical Predictions for the Spectral Tilt for Statistically Relevant Values of the Hamiltonian

Since the spectral tilts observed in Section 4 correspond to more energy at large scales and less energy at small scales, as in a spectrum for the Burgers equation associated with shock formation and nonlinear energy transfer, the skeptical reader

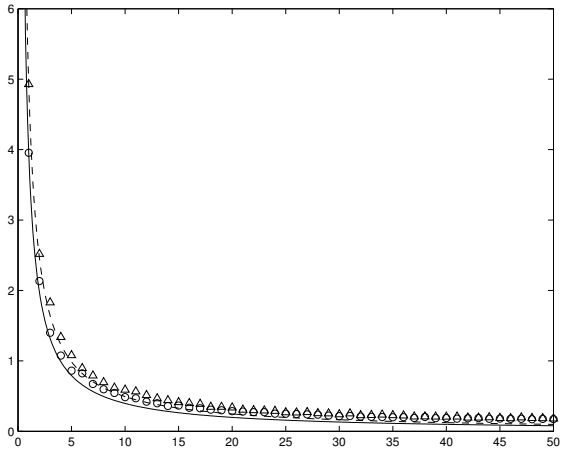

(a) Random initial data. Circles: $H = 8 \cdot 10^{-3}$; triangles: $H = 2 \cdot 10^{-3}$; solid line: fit $C\sqrt{\beta}/k$ for circles, $C = 0.1769$; dashed line: fit $C\sqrt{\beta}/k$ for triangles, $C = 0.2204$.

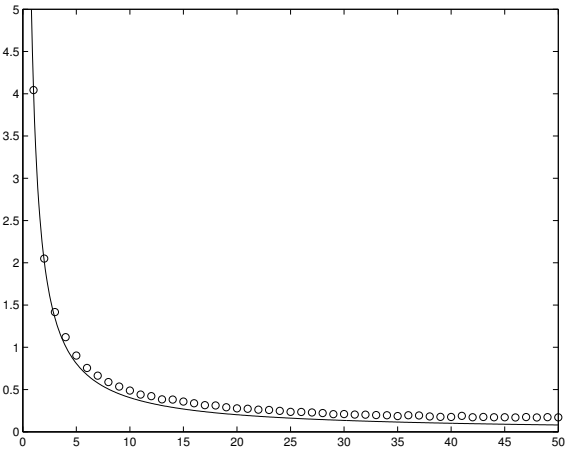

(b) $\sin(x) + \cos(2x)$ initial data. Circles: $H = 1.1 \cdot 10^{-2}$; solid line: fit $C\sqrt{\beta}/k$, $C = 0.1808$.

FIGURE 4.7. Correlation time scaling for (a) random and (b) deterministic initial data, $\Lambda = 50$, $E = 0.1$.

might attribute this behavior to numerical artifacts. Here we show that such concerns are unwarranted. In this section, we present a purely equilibrium statistical-mechanical Monte Carlo computation that predicts the spectral tilt seen in the numerical solutions of the truncated Burgers-Hopf equations (2.27) with statistically relevant initial data. Since all the statistics presented in the previous section were

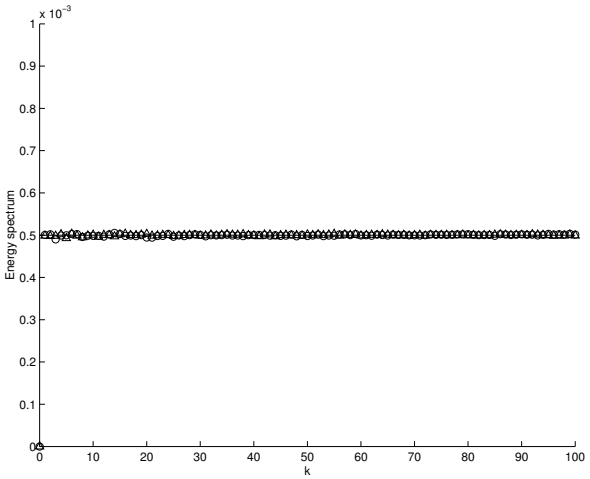

(a) Energy spectrum. Circles: $H = -1.1 \cdot 10^{-3}$; triangles: $H = -2.2 \cdot 10^{-3}$; horizontal line implies equipartitioned spectrum.

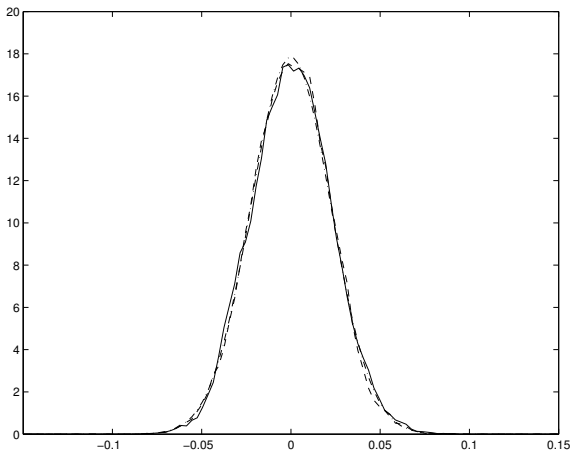

(b) PDF for mode $k = 1$. Solid line: $H = -1.1 \cdot 10^{-3}$; dashed line: $H = -2.2 \cdot 10^{-3}$; dash-dotted line: Gaussian fit with the same variance centered at zero.

FIGURE 4.8. (a) Energy spectrum and (b) PDF for random initial data, $\Lambda = 100$, $E = 0.1$.

gathered microcanonically by following long-time trajectories, here we also compute the energy spectra by using the microcanonical distribution in both the energy (2.29) and the Hamiltonian (2.26) in conjunction with a modification of the basic Monte Carlo algorithm discussed on page 18.

It is clear that this purely equilibrium statistical computation can only be successful if the computed trajectories are ergodic on the joint isosurfaces of the energy E and the Hamiltonian H, and, in fact, the remarkable agreement between

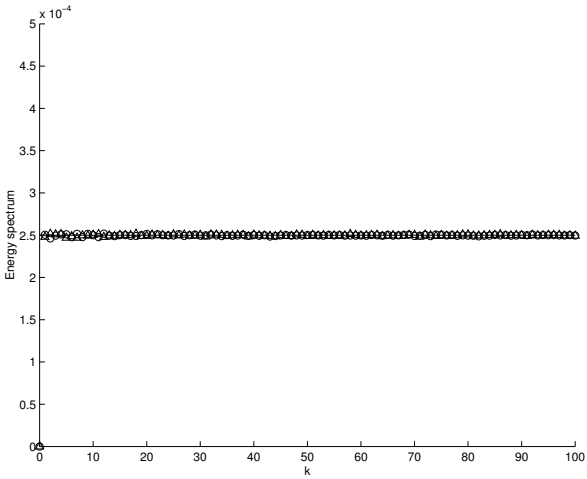

(a) Energy spectrum. Circles: $H = -6.3 \cdot 10^{-4}$; triangles: $H = 3.8 \cdot 10^{-5}$; horizontal line implies equipartitioned spectrum.

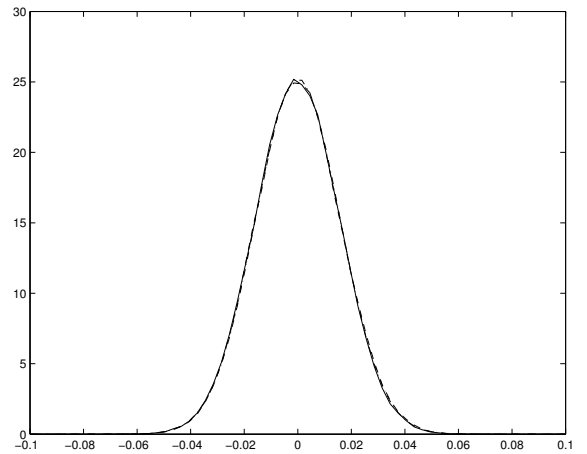

(b) PDF for mode $k = 1$. Solid line: $H = -6.3 \cdot 10^{-4}$; dashed line: $H = 3.8 \cdot 10^{-5}$; dash-dotted line: Gaussian fit with the same variance centered at zero.

FIGURE 4.9. (a) Energy spectrum and (b) PDF for random initial data, $\Lambda = 200$, $E = 0.1$.

the spectra computed from equilibrium statistical mechanics by the Monte Carlo method and those computed by direct numerical simulations provides additional strong numerical evidence that this ergodicity truly takes place.

We first compute the restriction of the measure (3.15) to the joint isosurface of the energy E in (2.29) and the Hamiltonian H in (2.26), $E = \bar{E}$ and $H = \bar{H}$, which is given by the formula

$$d\mu_{\bar{H},\bar{E},\Lambda} = \Gamma \delta(H(u_\Lambda) - \bar{H}) d\nu_{\bar{E},\Lambda}\,, \tag{5.1}$$

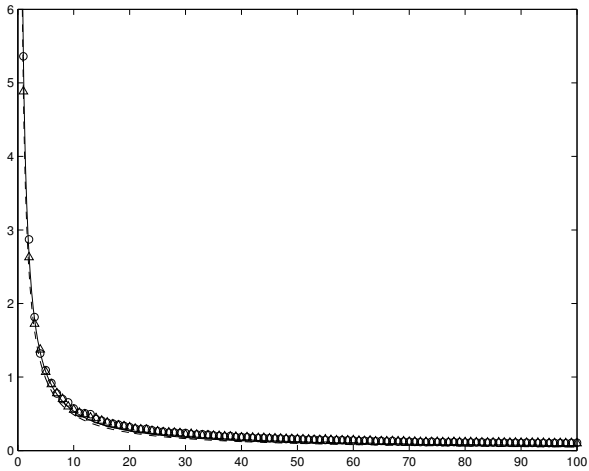

(a) Correlation times for random initial data, $\Lambda = 100$, $E = 0.1$. Circles: $H = -1.1 \cdot 10^{-3}$; triangles: $H = -2.2 \cdot 10^{-3}$; solid line: fit $C\sqrt{\beta}/k$ for circles, $C = 0.1695$; dashed line: fit $C\sqrt{\beta}/k$ for triangles, $C = 0.1544$.

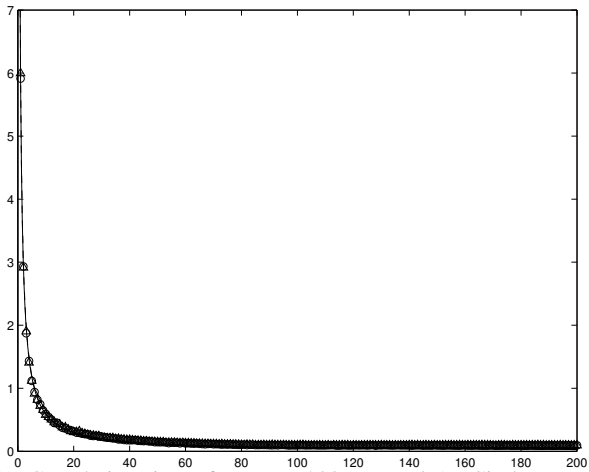

(b) Correlation times for $\Lambda = 200$, $E = 0.1$. Circles: $H = -6.3 \cdot 10^{-4}$; triangles: $H = 3.8 \cdot 10^{-5}$; solid line: fit $C\sqrt{\beta}/k$ for circles, $C = 0.1322$; dashed line: fit $C\sqrt{\beta}/k$ for triangles, $C = 0.1341$.

FIGURE 4.10. Correlation time scaling for (a) $\Lambda = 100$ and (b) $\Lambda = 200$, $E = 0.1$.

where Γ is a normalizing factor. The energy spectrum restricted to this isosurface is computed from the formula

$$\frac{1}{2}\langle|\hat{u}_k|^2\rangle = \frac{1}{2}\int\limits_{S_{\bar{E},\Lambda}} |\hat{u}_k|^2 \, d\mu_{\bar{H},\bar{E},\Lambda} \,. \tag{5.2}$$

The Monte Carlo algorithm of Section 3.2 for generating an approximately uniform distribution of points on the constant-energy sphere $S_{\bar{E},\Lambda}$ provides a good numerical approximation of the measure (3.15). Our task remains to include the numerical version of the term $\delta(H(u_\Lambda) - \bar{H})$ in (5.1).

To this end, we regularize the delta function $\delta(\lambda)$ by the expression

$$F_\varepsilon(\lambda) = \varepsilon^{-1}\chi_{A_\varepsilon}(\lambda) \quad \text{where } A_\varepsilon = \left\{\lambda : |\lambda| \le \frac{\varepsilon}{2}\right\} \tag{5.3}$$

and $\chi_S(x)$ is the characteristic function of the set S, as defined in formula (3.27). Since $F_\varepsilon(\lambda) \to \delta(\lambda)$ as $\varepsilon \to 0$, we can write an approximation for (5.2) as

$$\langle|\hat{u}_k|^2\rangle_\varepsilon = \frac{\int_{S_{\bar{E},\Lambda}} |\hat{u}_k|^2 F_\varepsilon[H(u_\Lambda) - \bar{H}]dv_{\bar{E},\Lambda}}{\int_{S_{\bar{E},\Lambda}} F_\varepsilon[H(u_\Lambda) - \bar{H}]dv_{\bar{E},\Lambda}}. \tag{5.4}$$

In practice, our Monte Carlo computation proceeds as follows: We first choose the truncation size Λ, the energy value $\bar{E}$, the value of the Hamiltonian $\bar{H}$, and a small ε. We then generate a sequence of vectors $(\hat{u}_1^{(i)}, \hat{u}_2^{(i)}, \ldots, \hat{u}_\Lambda^{(i)})$, $i = 1, 2, \ldots$, by using the Monte Carlo algorithm described on page 18 with $\bar{E}$ as the energy value. If $|H(u_\Lambda^{(i)}) - \bar{H}| \le \varepsilon/2$, the vector $(\hat{u}_1^{(i)}, \hat{u}_2^{(i)}, \ldots, \hat{u}_\Lambda^{(i)})$ is recorded. The recorded vectors are renumbered as $(\hat{u}_1^{(j)}, \hat{u}_2^{(j)}, \ldots, \hat{u}_\Lambda^{(j)})$, $j = 1, 2, \ldots, M$. The energy spectrum is then computed from the formula

$$\frac{1}{2}\langle|\hat{u}_k g|^2\rangle = \frac{1}{2M}\sum_{j=1}^{M} \left|\hat{u}_k^{(j)}\right|^2, \quad k = 1, 2, \ldots, \Lambda. \tag{5.5}$$

The convergence of this algorithm for fixed E in the limit as $M \to \infty$ to the true expected values (5.2) of the spectral coefficients on the slightly regularized joint isosurfaces of the energy and the Hamiltonian is guaranteed via the law of large numbers.

5.1 Comparison of Equilibrium Statistical Predictions and Direct Numerical Simulation for the Spectrum

In Figures 5.1 and 5.2, we present several examples of energy spectra of the truncated Burgers-Hopf equation (2.27) computed from (5.5) via the Monte Carlo algorithm described on page 18 and compared with the direct simulation. We have chosen the values of the energy $E = 0.1$ and the Hamiltonian $H = 1.1 \cdot 10^{-2}$. We compare the results of these Monte-Carlo-based spectral computations to direct simulations of the truncated Burgers-Hopf equations (2.27) with the initial condition $\sqrt{2E}(\sin x + \cos 2x)$. For this initial condition, the value of the energy is $E = 0.1$, and the value of the Hamiltonian is atypical, $H = 1.1 \cdot 10^{-2}$. For the Monte Carlo computations, we chose $\varepsilon = 10^{-4}$. The chosen truncation sizes are $\Lambda = 10$, $\Lambda = 20$, and $\Lambda = 50$. In all the direct simulations, the time

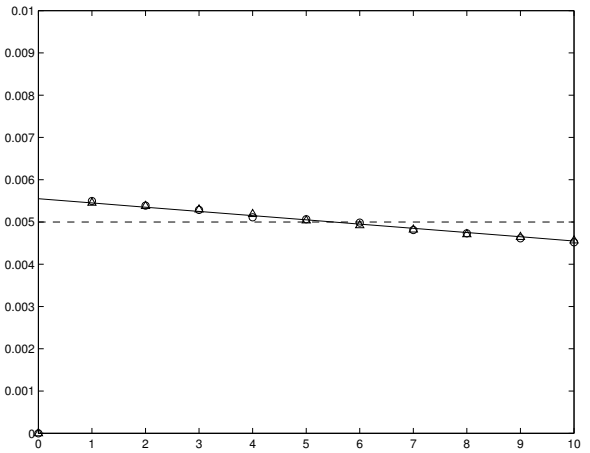

(a) $\Lambda = 10$. Circles: Burgers-Hopf; triangles: Monte Carlo; solid line shows the analytical fit; dashed horizontal line implies equipartitioned spectrum.

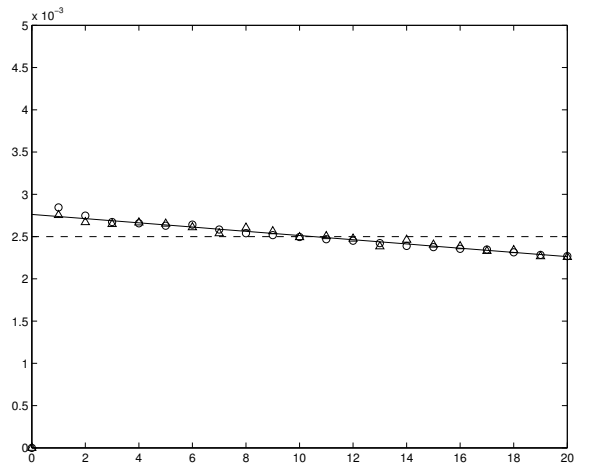

(b) $\Lambda = 20$. Circles: Burgers-Hopf; triangles: Monte Carlo, solid line shows the analytical fit; dashed horizontal line implies equipartitioned spectrum.

FIGURE 5.1. Energy spectra for $E = 0.1$, $H = 1.1 \cdot 10^{-2}$, computed from the solution of the Burgers-Hopf truncation with deterministic initial data $\sqrt{2E}(\sin(x) + \cos(2x))$ and from the Monte Carlo simulation for (a) $\Lambda = 10$ and (b) $\Lambda = 20$.

step is $\Delta t = 10^{-3}$, the initial averaging time is $T_0 = 1000$, the averaging window $T = 20000$, the energy (2.29) is conserved within $10^{-8}\%$, and the Hamiltonian (2.26) within $10^{-9}\%$.

As we can see from Figures 5.1 and 5.2, the results of the equilibrium Monte Carlo computations and the direct truncated Burgers-Hopf simulations both yield

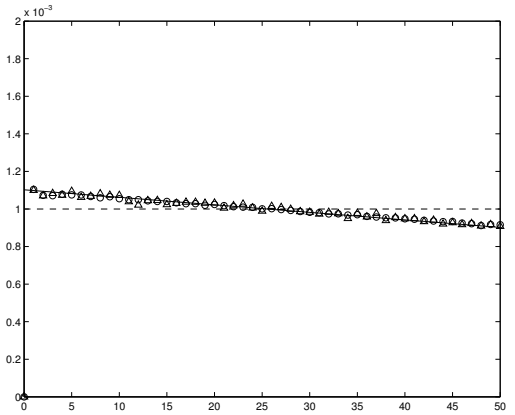

FIGURE 5.2. Energy spectra computed from the solution of the Burgers-Hopf truncation with deterministic initial data $\sqrt{2E}(\sin(x) + \cos(2x))$ and from the Monte Carlo simulation for $\Lambda = 50$, $E = 0.1$, $H = 1.1 \cdot 10^{-2}$. Circles: Burgers-Hopf; triangles: Monte Carlo; solid line shows the analytical fit; dashed horizontal line implies equipartitioned spectrum.

spectral tilts that are in excellent agreement. In particular, their maximal mutual relative error is 3.23%. This agreement provides a clear numerical confirmation of the accuracy of our equilibrium Monte Carlo predictions in the microcanonical setting, as well as a clear validation of the assumption that the trajectories of the truncated Burgers-Hopf equations (2.27) are ergodic on the joint isosurfaces of the energy and the Hamiltonian.

The computed energy spectra for the atypical values of the Hamiltonian H shown in Section 4 and the preceding paragraph, and the values of the spectral tilt displayed in Table 4.2 furnish strong numerical evidence for the following characteristics of the tilt:

- The tilt is a linear function of the mode number k, and the spectral values decrease with increasing k.
- The spectrum is tilted about the point $(\Lambda + 1)/2$, where it crosses the horizontal line at $E_{p/m}(\Lambda) = E/2\Lambda$, which is the mean energy per mode predicted by the equipartition formula (3.7).

5.2 A Heuristic Universal Formula for the Spectral Tilt

By using these two observations, here we propose a heuristic formula for quantifying the tilt in the energy spectrum

$$\frac{1}{2}\langle|\hat{u}_k|^2\rangle = E_{p/m}(\Lambda)\left(1 + \alpha(E, H)\frac{(\Lambda + 1)/2 - k}{\Lambda}\right), \tag{5.6}$$

where $\alpha(E, H)$ is a function that we now determine. Note that, since

$$\sum_{k=1}^{\Lambda} \left[\frac{\Lambda + 1}{2} - k \right] = 0$$

for all truncation sizes Λ, the terms multiplied by $\alpha(E, H)$ do not affect the total energy.

In all three cases presented in the paragraphs above, we find the parameter $\alpha(E, H)$ to be

$$\alpha(E, H) = 0.2\,.$$

We thus conclude that $\alpha(E, H)$ is independent of the truncation size Λ.

Since $H = 0$ is an irrelevant value and no tilt occurs for it, $\alpha(E, H)$ must satisfy

$$\alpha(E, 0) = 0\,,$$

and since $\alpha(E, H)$ is nondimensional, we must have

$$\alpha(E, H) = \alpha\left(\frac{H^2}{E^3}\right)$$

for some nonlinear function α. For $(H^2/E^3) \ll 1$, which is true in all our computations, we can Taylor-expand $\alpha(H^2/E^3)$ and only keep the first term,

$$\alpha(E, H) = \mu \frac{H^2}{E^3}\,. \tag{5.7}$$

Thus, the expression (5.6) finally becomes

$$\frac{1}{2}\left\langle |\hat{u}_k|^2 \right\rangle = E_{p/m}(\Lambda)\left(1 + \mu \frac{H^2}{E^3} \frac{(\Lambda + 1)/2 - k}{\Lambda}\right). \tag{5.8}$$

Assuming the form (5.7) of $\alpha(E, H)$, we have revisited the numerical experiments of Section 4, in which the energy is fixed at $E = 0.1$, whereas the values of the Hamiltonian H vary from $3 \cdot 10^{-3}$ to $1.1 \cdot 10^{-2}$, and the values of Λ vary from 10 to 200. From these experiments we determine that μ is also constant within about 5%, i.e.,

$$\mu = 1.60438 \pm 8.031 \cdot 10^{-2}\,.$$

Thus, the heuristic formula in (5.8) provides an excellent fit for all of the spectral tilts that have been observed in numerical simulations throughout this paper for $E = 0.1$. Also, this formula is completely self-consistent with the fact that no spectral tilt occurs for statistically irrelevant values of the Hamiltonian.

6 Concluding Discussion

The results in this paper, which were established through a combination of numerical simulations of the truncated Burgers-Hopf equation, Monte Carlo simulations for equilibrium ensembles, and simple mathematical arguments, suggest several new problems in equilibrium statistical mechanics that merit further study through completely rigorous mathematical analysis. The first of these is a central limit theorem for the probability density of the Hamiltonian on a microcanonical energy surface for both of the limits for either fixed mean energy or fixed mean energy per mode as $\Lambda \to \infty$. The second main problem involves a suitable large-deviation principle for the statistically relevant values of H that confirm the spectral tilt seen in both the simulations and confirmed by the equilibrium statistical Monte Carlo simulations in Section 5. A rigorous proof of the heuristic formula for this spectral tilt for Section 5 for finite Λ or a suitable generalization would also be very interesting.

In this paper, we have emphasized the behavior as Λ increases with fixed mean energy. This is the natural one for geophysical applications. The behavior in the thermodynamic limit where the energy per mode is fixed and Λ increases is also very interesting, and results for this case can be found in [2] and will be reported elsewhere.

Acknowledgments. The authors thank Peter Lax for his interest in this work. They also thank Jonathan Goodman for suggesting the Monte Carlo algorithm used in this paper during a conversation with A. Majda in the 13^{th}-floor lounge at CIMS; the authors' original version was a poor man's version of the same algorithm. Moreover, the authors thank Ilya Timofeyev for stimulating conversations about this work. A. Majda is partially supported by grants from ONR, ARO, and NSF. G. Kovačič was partially supported by an NSF CAREER grant. R. Abramov is supported as a research assistant on Majda's NSF grant and was previously supported as a research assistant on Kovačič's NSF CAREER grant.

Bibliography

[1] Abraham, R.; Marsden, J. E. *Foundations of mechanics.* Second edition. Benjamin/Cummings, Reading, Mass., 1978.

[2] Abramov, R. V. Statistically relevant and irrelevant conserved quantities for the equilibrium statistical description of the truncated Burgers-Hopf equation and the equations for barotropic flow. Doctoral dissertation, Rensselaer Polytechnic Institute, 2002.

[3] Abramov, R. V.; Majda, A. J. Statistically relevant conserved quantities for truncated quasi-geostrophic flow. In preparation.

[4] Arnol′d, V. I. *Mathematical methods of classical mechanics*. Second edition. Graduate Texts in Mathematics, 60. Springer, New York, 1989.

[5] Ascher, U. M.; Petzold, L. R. *Computer methods for ordinary differential equations and differential-algebraic equations.* Society for Industrial and Applied Mathematics (SIAM), Philadelphia, 1998.

[6] Carnevale, G. F.; Frederiksen, J. S. Nonlinear stability and statistical mechanics of flow over topography. *J. Fluid Mech.* **175** (1987), 157–181.

[7] Gardner, C. S. Korteweg–de Vries equation and generalizations. IV. The Korteweg–de Vries equation as a Hamiltonian system. *J. Mathematical Phys.* **12** (1971), 1548–1551.

[8] Holloway, G. Eddies, waves, circulation, and mixing: statistical geofluid mechanics. *Annual review of fluid mechanics*, **18**, 91–147. Annual Reviews, Palo Alto, Calif., 1986.

[9] Kleeman, R.; Majda, A. J.; Timofeyev, I. Quantifying predictability in a model with statistical features of the atmosphere. *Phys. D*, in press.

[10] Lamperti, J. W. *Probability*. A survey of the mathematical theory. Benjamin, New York–Amsterdam, 1966.

[11] Lasota, A.; Mackey, M. C. *Chaos, fractals, and noise.* Stochastic aspects of dynamics. Second edition. Applied Mathematical Sciences, 97. Springer, New York, 1994.

[12] Majda, A. J.; Timofeyev, I. Remarkable statistical behavior for truncated Burgers-Hopf dynamics. *Proc. Natl. Acad. Sci. USA* **97** (2000), no. 23, 12413–12417.

[13] Majda, A. J.; Timofeyev, I. Statistical mechanics for truncations of the Burgers-Hopf equation. A model for intrinsic stochastic behavior with scaling. *Milan J. Math.* **70** (2002), no. 1, 39–96.

[14] Majda, A. J.; Timofeyev, I.; Vanden Eijnden, E. A mathematical framework for stochastic climate models. *Comm. Pure Appl. Math.* **54** (2001), no. 8, 891–974.

[15] Majda, A. J.; Timofeyev, I.; Vanden Eijnden, E. A priori tests of a stochastic mode elimination strategy. *Phys. D*, in press.

[16] Majda, A. J.; Wang, X. *Nonlinear dynamics and statistical theories for basic geophysical flows.* Cambridge University Press, forthcoming.

[17] Morrison, P. J. Hamiltonian description of the ideal fluid. *Rev. Modern Phys.* **70** (1998), no. 2, 467–521.

[18] Salmon, R. *Lectures on geophysical fluid dynamics.* Oxford University Press, New York, 1998.

[19] Turkington, B.; Majda, A.; Haven, K.; DiBattista, M. Statistical equilibrium predictions of jets and spots on Jupiter. *Proc. Natl. Acad. Sci. USA* **98** (2001), no. 22, 12346–12350.

RAFAIL V. ABRAMOV
Courant Institute
251 Mercer Street
New York, NY 10012-1185
E-mail: abramov@cims.nyu.edu

GREGOR KOVAČIČ
Rensselaer Polytechnic Institute
Department of Mathematics
110 8th Street
Troy, NY 12180
E-mail: kovacg@rpi.edu

ANDREW J. MAJDA
Courant Institute
251 Mercer Street
New York, NY 10012-1185

Received December 2001.
Revised July 2002.